

A global analysis of axion-like particle interactions using SMEFT fits

Anke Biekötter^a, Javier Fuentes-Martín^b, Anne Mareike Galda^a and Matthias Neubert^{a,c}

^a*PRISMA⁺ Cluster of Excellence & Mainz Institute for Theoretical Physics
Johannes Gutenberg University, 55099 Mainz, Germany*

^b*Departamento de Física Teórica y del Cosmos, Universidad de Granada,
Campus de Fuentenueva, E-18071 Granada, Spain*

^cDepartment of Physics, LEPP, Cornell University, Ithaca, NY 14853, U.S.A.

Abstract

In the presence of an axion or axion-like particle (ALP) that couple to the Standard Model via dimension-five interactions, dimension-six SMEFT interactions are generated via renormalization-group evolution. As many of these SMEFT contributions are experimentally tightly constrained, this “ALP–SMEFT interference” can be used to derive indirect bounds on the ALP couplings to the Standard Model particles. We present a global analysis of the Wilson coefficients of the ALP effective Lagrangian based on Higgs, top, and low-energy data. The obtained bounds are model independent and are competitive or even stronger than direct bounds in the GeV to TeV ALP-mass range.

Contents

1	Introduction	1
2	ALP couplings to the SM	2
2.1	The ALP Lagrangian	2
2.2	ALP–SMEFT interference	4
2.3	Solving the ALP–SMEFT RG equations	4
3	Global analysis of ALP couplings	5
3.1	Experimental inputs and SMEFT predictions	5
3.2	Fit results	6
3.3	Comparison with bounds from direct searches	10
4	Interpretation in terms of UV-complete models	12
4.1	KSVZ model	12
4.2	DFSZ model	14
5	Conclusions	17
A	Experimental inputs	19
B	Contributions to Z-pole observables in the LL approximation	22

1 Introduction

The lack of new-particle discoveries at the Large Hadron Collider (LHC) other than the Higgs boson restricts the space of possibilities for physics beyond the Standard Model (SM). To have evaded detection so far, new particles must either be too heavy to be produced in current high-energy experiments, or interact very weakly with the SM particles. Pseudo Nambu–Goldstone bosons that appear from the spontaneous breaking of a global symmetry, commonly referred to as axions and axion-like particles (ALPs), are among the best motivated light particles beyond the SM. They could play a crucial role in the solution to the strong CP problem [1–3] and are potential dark matter candidates (see [4] for a review). While most explicit models addressing the strong CP problem predict a strict relation between the axion mass and its decay constant, it is also possible to obtain solutions to the strong CP problem with heavier axions [5–17]. Furthermore, composite-Higgs models [18, 19] and even supersymmetric extensions of the SM [20–22] naturally give rise to ALPs. These models provide a good motivation to search for light pseudoscalar particles in a parameter space that extends beyond the traditional axion searches. Indeed, one of the main interests in searching for ALPs is that they can be a forerunner of a high-scale new physics sector, which otherwise could be hard to access experimentally.

Direct ALP searches span from cosmological [23, 24] and astrophysical [25, 26] observations to collider [27–32] and flavor [33–38] experiments. These observables impose powerful constraints on the ALP parameter space, although often under very specific assumptions on its interactions. For example, direct searches for ALPs at particle colliders must make an assumption about the process in which the ALP is produced (e.g. in the decay of a Higgs boson, and Z boson, or in weak decays of kaons or B mesons), about its lifetime, and the way in which it decays, which may involve a decay outside of the detector. In the derivation of astrophysical bounds on, e.g., the ALP–photon

coupling from supernovae or ALPs produced in the sun, it makes a crucial difference whether or not a vanishing ALP–electron coupling is assumed. In the vast majority of the existing analyses, it was assumed that only a single ALP couplings is non-zero at the scale of Peccei–Quinn symmetry breaking – an assumption which is not valid in even the classic KSVZ [39, 40] and DFSZ [41, 42] models for the QCD axion.

As recently shown in [43], the presence of ALP couplings to SM particles yields a non-trivial renormalization-group (RG) flow into the Wilson coefficients of the dimension-six Standard Model Effective Field Theory (SMEFT) operators. This opens up the interesting possibility of indirectly testing ALP interactions by utilizing existing SMEFT studies. In this paper, we exploit the ALP–SMEFT interference to deduce constraints from a global fit including low-energy, Higgs and top data, as implemented in current global SMEFT analyses [44–62], thus providing a complementary use of these observables to constrain light new physics. As we show, our analysis probes previously unexplored parts of the ALP parameter space, especially for ALP masses above 10 GeV. Furthermore, one of the significant advantages of our indirect approach is that the derived bounds are mostly independent of the ALP mass and require no assumptions on other ALP couplings or the ALP lifetime. This feature overcomes one of the main limitations of direct ALP searches, which often produce highly model-dependent constraints. Therefore, the indirect ALP bounds presented in this paper offer an important complementary approach with respect to direct constraints even when the latter appear to be stronger under certain conditions.

This paper is organized as follows: Section 2 introduces the ALP–SMEFT Lagrangian and discusses its connection to the SMEFT. In Section 3, we describe the global analysis setup, present the fit results and compare them to bounds from direct searches. Section 4 is dedicated to a reinterpretation of our global analysis in terms of concrete ultraviolet (UV) completions. We conclude in Section 5.

2 ALP couplings to the SM

We consider an extension of the SM that includes a pseudoscalar, gauge-singlet ALP as an additional light state. Its couplings to SM fields are, at the classical level, protected by an approximate shift symmetry $a \rightarrow a + c$, broken softly by the ALP mass term m_a . We relegate the discussion of possible UV completions of this model to Section 4.

2.1 The ALP Lagrangian

It has been pointed out in [43] that a consistent effective field theory (EFT) for an extension of the SM featuring an ALP must necessarily include higher-dimensional operators built out of SM fields only. Above the electroweak scale, the most general effective Lagrangian describing the interactions of an ALP with SM particles thus reads

$$\mathcal{L} = \frac{1}{2} (\partial_\mu a)(\partial^\mu a) - \frac{m_a^2}{2} a^2 + \mathcal{L}_{\text{SM+ALP}} + \mathcal{L}_{\text{SMEFT}}, \quad (1)$$

with $\mathcal{L}_{\text{SMEFT}}$ denoting the SMEFT Lagrangian. The SMEFT Lagrangian up to dimension-six order can be found in [63]. In what follows, we adopt the same conventions as in this reference, except for the labels for the Higgs field and its (tachyonic) mass, for which we use H and m_H , respectively. Note, in particular, that we work with dimensionless Wilson coefficients and factor out inverse powers of the new-physics scale Λ when writing down higher-dimensional operators in the effective Lagrangian. The Lagrangian $\mathcal{L}_{\text{SM+ALP}}$ describes the ALP interactions with SM particles. Apart

from the soft symmetry breaking by the ALP mass m_a , we consider only classically shift-invariant interactions with the SM fields. Specifically, the ALP Lagrangian up to dimension-six operators is then given by¹

$$\begin{aligned} \mathcal{L}_{\text{SM+ALP}}^{D\leq 6} = & c_{GG} \frac{a}{f} \frac{\alpha_s}{4\pi} G_{\mu\nu}^A \tilde{G}^{\mu\nu A} + c_{WW} \frac{\alpha_L}{4\pi} \frac{a}{f} W_{\mu\nu}^I \tilde{W}^{\mu\nu I} + c_{BB} \frac{\alpha_Y}{4\pi} \frac{a}{f} B_{\mu\nu} \tilde{B}^{\mu\nu} \\ & + \frac{\partial^\mu a}{f} \sum_F \bar{F} \mathbf{c}_F \gamma_\mu F + \frac{c_{HH}}{f^2} (\partial^\mu a)(\partial_\mu a) H^\dagger H, \end{aligned} \quad (2)$$

where \mathbf{c}_F ($F = q, u, d, l, e$) are 3×3 hermitian matrices and c_{ii} ($i = G, W, B, H$) are real couplings. The real parameter f is referred to as the ALP decay constant, which is related to the relevant new-physics scale by

$$\Lambda = 4\pi f. \quad (3)$$

The Lagrangian above can be cast into an alternative but equivalent form, in which the ALP couplings to fermions are of non-derivative type. This is achieved by means of the field redefinitions $F \rightarrow F + i \frac{a}{f} \mathbf{c}_F F$ in (1), which yields

$$\begin{aligned} \mathcal{L}_{\text{SM+ALP}}^{D\leq 6} \rightarrow & C_{GG} \frac{a}{f} G_{\mu\nu}^A \tilde{G}^{\mu\nu A} + C_{WW} \frac{a}{f} W_{\mu\nu}^I \tilde{W}^{\mu\nu I} + C_{BB} \frac{a}{f} B_{\mu\nu} \tilde{B}^{\mu\nu} \\ & - \frac{a}{f} \left(\bar{q} \tilde{H} \tilde{\mathbf{Y}}_u u_R + \bar{q} H \tilde{\mathbf{Y}}_d d_R + \bar{l} H \tilde{\mathbf{Y}}_e e_R + \text{h.c.} \right) \\ & + \frac{1}{2} \frac{a^2}{f^2} \left(\bar{q} \tilde{H} \mathbf{Y}'_u u_R + \bar{q} H \mathbf{Y}'_d d_R + \bar{l} H \mathbf{Y}'_e e_R + \text{h.c.} \right) + \frac{c_{HH}}{f^2} (\partial^\mu a)(\partial_\mu a) H^\dagger H. \end{aligned} \quad (4)$$

Note that due to the axial anomaly, additional contributions enter the ALP couplings to gauge bosons, such that c_{VV} and C_{VV} are related by [64]

$$\begin{aligned} C_{GG} &= \frac{\alpha_s}{4\pi} \left[c_{GG} + \frac{1}{2} \text{Tr}(\mathbf{c}_d + \mathbf{c}_u - 2\mathbf{c}_q) \right], \\ C_{WW} &= \frac{\alpha_L}{4\pi} \left[c_{WW} - \frac{1}{2} \text{Tr}(N_c \mathbf{c}_q + \mathbf{c}_l) \right], \\ C_{BB} &= \frac{\alpha_Y}{4\pi} \left[c_{BB} + \text{Tr} \left(N_c (\mathcal{Y}_d^2 \mathbf{c}_d + \mathcal{Y}_u^2 \mathbf{c}_u - 2\mathcal{Y}_q^2 \mathbf{c}_q) + \mathcal{Y}_e^2 \mathbf{c}_e - 2\mathcal{Y}_l^2 \mathbf{c}_l \right) \right], \end{aligned} \quad (5)$$

with $N_c = 3$ and the hypercharges $\mathcal{Y}_u = 2/3$, $\mathcal{Y}_d = -1/3$, $\mathcal{Y}_q = 1/6$, $\mathcal{Y}_e = -1$, $\mathcal{Y}_l = -1/2$. The new ALP-fermion coupling matrices are related to the original Lagrangian couplings by

$$\begin{aligned} \tilde{\mathbf{Y}}_{F_R} &= i (\mathbf{Y}_{F_R} \mathbf{c}_{F_R} - \mathbf{c}_{F_L} \mathbf{Y}_{F_R}), \\ \mathbf{Y}'_{F_R} &= \mathbf{c}_{F_L}^2 \mathbf{Y}_{F_R} - 2 \mathbf{c}_{F_L} \mathbf{Y}_{F_R} \mathbf{c}_{F_R} + \mathbf{Y}_{F_R} \mathbf{c}_{F_R}^2, \end{aligned} \quad (6)$$

with $F_R = u, d, e$ and $F_L = q(l)$ for quark (lepton) couplings. Assuming a flavor-universal structure for the \mathbf{c}_F couplings, i.e. $\mathbf{c}_F = c_F \mathbb{1}_3$, these interactions reduce to

$$\tilde{\mathbf{Y}}_{F_R} = i \mathbf{Y}_{F_R} C_{F_R}, \quad \mathbf{Y}'_{F_R} = \mathbf{Y}_{F_R} C_{F_R}^2, \quad (7)$$

where $C_{u,d} \equiv c_{u,d} - c_q$ and $C_e \equiv c_e - c_l$. In the flavor-universal scenario, dimension-five ALP interactions with SM particles are thus fully described by six free parameters: C_{GG} , C_{WW} , C_{BB} , C_u , C_d and C_e .²

¹We do not include redundant operators such as $\partial^\mu a (H^\dagger i \overleftrightarrow{D}_\mu H)$, which can be rewritten in terms of the ones here by means of field redefinitions [64].

²Given the hierarchical structure of the SM Yukawas, similar leading-order interactions would also be obtained for other flavor hypotheses in which third-family interactions are not (strongly) suppressed. The fermionic couplings $C_{u,d,e}$ correspond to the couplings c_{ff} in [43] in flavor-universal scenarios, e.g. $C_u = c_{uu} = c_{cc} = c_{tt}$.

2.2 ALP – SMEFT interference

The dimension-five ALP couplings to SM particles generate divergent amplitudes that require dimension-six SMEFT counterterms. As a result, the RG equations for the SMEFT operators get modified by additional inhomogeneous source terms, such that the scale dependence in the presence of the ALP is given by

$$\frac{d}{d \ln \mu} C_i^{\text{SMEFT}} - \gamma_{ji}^{\text{SMEFT}} C_j^{\text{SMEFT}} = \gamma_{i\alpha\beta}^{\text{SMEFT-ALP}} C_\alpha^{\text{ALP}} [C_\beta^{\text{ALP}}]^*. \quad (8)$$

Here γ^{SMEFT} denotes the anomalous-dimension matrix of the dimension-six SMEFT operators calculated in [65–68], and the source terms $\gamma^{\text{SMEFT-ALP}}$ have been calculated in [43].³ The presence of ALP interactions with the SM particles thus generates a non-trivial RG flow into the SMEFT Wilson coefficients. The dimension-six inhomogeneous source terms are independent of the ALP mass. Thus, as long as the ALP mass lies below the scale of the observables used in the fit, we will obtain mass-independent indirect bounds on the ALP couplings.

In addition to the contributions to the RG equations of the dimension-six SMEFT operators, the presence of the ALP also introduces modifications to the running of dimension-four couplings. Most of these modifications were discussed in [43]. However, additional contributions arise from the dimension-six operators included in (4), which we present here for the first time. They are

$$\frac{d\mathbf{Y}_{u,d,e}}{d \ln \mu} \supset -\frac{m_a^2}{2\Lambda^2} \mathbf{Y}'_{u,d,e}, \quad \frac{dm_H^2}{d \ln \mu} \supset \frac{m_a^4}{\Lambda^2} c_{HH}, \quad (9)$$

where again $\Lambda = 4\pi f$.

2.3 Solving the ALP – SMEFT RG equations

The RG equations for the ALP – SMEFT Lagrangian can generically be written as⁴

$$\begin{aligned} \frac{dC_a^{(4)}(t)}{dt} &= \gamma_{ba}^{(4)}(\mathbf{C}^{(4)}, \mathbf{C}^{(5)}, \mathbf{C}^{(6)}) C_b^{(4)}(t), \\ \frac{dC_\alpha^{(5)}(t)}{dt} &= \gamma_{\beta\alpha}^{(5)}(\mathbf{C}^{(4)}) C_\beta^{(5)}(t), \\ \frac{dC_i^{(6)}(t)}{dt} &= \gamma_{ji}^{(6)}(\mathbf{C}^{(4)}) C_j^{(6)}(t) + \gamma_{i\alpha\beta}^{(5,5)}(\mathbf{C}^{(4)}) C_\alpha^{(5)}(t) [C_\beta^{(5)}(t)]^*, \end{aligned} \quad (10)$$

where $t \equiv \ln \mu$, and we have collected the Wilson coefficients into vectors $\mathbf{C}^{(D)}$, with the superscript denoting the dimension of the associated operator, and the indices a, b (for $D = 4$), α, β (for $D = 5$), and i, j (for $D = 6$) labeling the corresponding coefficients. $\gamma^{(D)}$ are the corresponding anomalous-dimension matrices, and $\gamma^{(5,5)}$ is the tensor accounting for the ALP source terms. The RG equations above form a system of coupled differential equations, for which an analytical solution is not known. One would thus be forced to solve this system numerically for a given set of initial conditions. It helps, however, to note that the RG equations above contain terms that are beyond dimension-six order in the EFT expansion. Indeed, using that $\mathbf{C}^{(4)}(t) = \mathbf{C}^{\text{SM}}(t) + \mathcal{O}(\Lambda^{-2})$, with \mathbf{C}^{SM} being the

³We follow the same conventions as in [63], implying a factor of 1/2 difference in the definition of λ when compared to [66–68], and a sign difference in the covariant derivatives relative to [43].

⁴The anomalous-dimension matrix $\gamma^{(5)}$ has been calculated in [64, 69, 70]. Numerical solutions to the corresponding RG equations can be obtained with the `ALPRunner` package [71].

SM couplings, we can rewrite the RG equations for the Wilson coefficients of the higher-dimensional operators in the form

$$\begin{aligned}\frac{dC_\alpha^{(5)}(t)}{dt} &= \gamma_{\beta\alpha}^{(5)}(\mathbf{C}^{\text{SM}}) C_\beta^{(5)}(t), \\ \frac{dC_i^{(6)}(t)}{dt} &= \gamma_{ji}^{(6)}(\mathbf{C}^{\text{SM}}) C_j^{(6)}(t) + \gamma_{i\alpha\beta}^{(5,5)}(\mathbf{C}^{\text{SM}}) C_\alpha^{(5)}(t) [C_\beta^{(5)}(t)]^*,\end{aligned}\tag{11}$$

in which all power-suppressed terms have been expanded out consistently. This system of equations admits an analytic solution for $\mathbf{C}^{(5,6)}(t)$ in terms of $\mathbf{C}^{\text{SM}}(t)$.⁵ Explicitly, we find

$$\begin{aligned}C_\alpha^{(5)}(t_f) &= U_{\alpha\beta}^{(5)}(t_f, t_0) C_\beta^{(5)}(t_0), \\ C_i^{(6)}(t_f) &= U_{ij}^{(6)}(t_f, t_0) C_j^{(6)}(t_0) + U_{i\alpha\beta}^{(5,5)}(t_f, t_0) C_\alpha^{(5)}(t_0) [C_\beta^{(5)}(t_0)]^*,\end{aligned}\tag{12}$$

where t_0 and t_f denote the logarithms of the initial and final energy scales, respectively, and the evolution tensors are defined as

$$\begin{aligned}U^{(D)}(t_f, t_0) &\equiv \mathcal{T} \exp \left[\int_{t_0}^{t_f} [\gamma^{(D)}(\mathbf{C}^{\text{SM}}(w))]^T dw \right], \\ U_{i\alpha\beta}^{(5,5)}(t_f, t_0) &\equiv U_{ij}^{(6)}(t_f, t_0) \int_{t_0}^{t_f} U_{jk}^6(t_0, w) \gamma_{k\rho\sigma}^{(5,5)}(\mathbf{C}^{\text{SM}}(w)) U_{\rho\alpha}^{(5)}(w, t_0) [U^{(5)}(w, t_0)_{\sigma\beta}]^*,\end{aligned}\tag{13}$$

with \mathcal{T} indicating that the exponential is t -ordered. Obtaining the evolution tensors is computationally expensive; however, they do not depend on the initial conditions set on the higher-dimensional operators and only need to be determined once (for a given set of SM input parameters). Once the evolution tensors are known, the computation of the running of the Wilson coefficients for arbitrary initial conditions is very fast.

The evolution matrix $U^{(6)}$ for the SMEFT has already been determined and is part of the computer tool `DsixTools` 2.0 [72, 73]. We have used a customized version of `DsixTools`, in which we have incorporated the ALP contributions to the RG equations, to compute the evolution tensor $U^{(5,5)}$ in the flavor-universal scenario. We provide this tensor for the SMEFT Wilson coefficients relevant for our fits in a `Mathematica` notebook as ancillary material. A new version of `DsixTools` featuring generic ALP contributions will be presented in a forthcoming paper.

3 Global analysis of ALP couplings

In the following, we utilize the ALP–SMEFT interference to derive (almost) mass-independent bounds on the ALP couplings to SM particles. Contrary to the direct bounds derived elsewhere, the results we obtain are model-independent in the framework we consider, consisting of an ALP added to the SM without additional sources of new physics. One of the advantages of this approach is that it lets us efficiently reuse results from existing SMEFT analyses.

3.1 Experimental inputs and SMEFT predictions

Limits on the SMEFT Wilson coefficients have been derived from a multitude of observables, including low-energy, Higgs and top data. For our global analysis, we utilize existing parametrizations of

⁵Note that the running of $\mathbf{C}^{(4)}$ up to dimension-six order still needs to be determined numerically for each set of initial conditions. However, the system of equations to be solved is now considerably smaller.

these observables in terms of the SMEFT Wilson coefficients and recast them in terms of ALP Wilson coefficients at the high-energy scale Λ . All of the SMEFT predictions used here are truncated at linear order in the dimension-six Wilson coefficients and employ $\{G_F, \alpha, M_Z\}$ as the electroweak input parameters.

Predictions for the Higgs sector are taken from [56] and references therein, while SMEFT predictions for the top sector are taken from `fitmaker` [55] and references therein. The experimental observables used for Higgs and top data are summarized in Tables 1-3 in Appendix A. The assumption of flavor universality in some SMEFT parametrizations of these observables, such as the ones from the experimental analysis in [74], causes certain complications, as ALP contributions are generally flavor-dependent. To overcome this issue, we will assume that the effects from operators involving quark couplings to gluons or the Higgs boson are dominated by those involving third-generation quarks, i.e.

$$C_{uG} \rightarrow [C_{uG}]_{33}, \quad C_{uH} \rightarrow [C_{uH}]_{33}, \quad C_{dH} \rightarrow [C_{dH}]_{33}, \quad (14)$$

where the notation $[C_x]_{ij}$ is used to denote the flavor indices i and j of the Wilson coefficient C_x . The constraints on the remaining operators with flavor indices are typically experimentally dominated by first- and second-generation couplings. We therefore take a conservative approach and assume pure second-generation contributions for these operators in the considered Higgs and top observables, e.g. $C_{Hl}^{(3)} \rightarrow [C_{Hl}^{(3)}]_{22}$.

We perform a χ^2 fit for the experimental data \vec{d} with the theory predictions $\vec{p}(C_i)$ and covariance matrix \mathbf{V} , using the definition

$$\chi^2(C_i) = [\vec{d} - \vec{p}(C_i)]^T \mathbf{V}^{-1} [\vec{d} - \vec{p}(C_i)]. \quad (15)$$

For low-energy observables including electroweak precision data, neutrino scattering, atomic parity violation and quark pair-production at LEP2, we directly use the χ^2 function provided in [44, 75], which includes the full flavor structure of the SMEFT Wilson coefficients.⁶

The SMEFT predictions are translated to ALP predictions using the solution to the RG equations in (12) for $C_i^{(6)}(t_0) = 0$, i.e. neglecting possible matching contributions at the high scale. The value of the high-scale is set to $\mu_0 = \Lambda = 4\pi f$, and the low-energy scale is identified with the relevant experimental scale for each of the observables, $\mu_f = \mu_{\text{exp}}$, with e.g. $\mu_{\text{exp}} = m_h$ for gluon-fusion Higgs production observables and $\mu_{\text{exp}} = m_h + 2m_t$ for $t\bar{t}h$ production. When considering ALP masses above the Z mass, as we will do in Section 3.3, we stop the ALP-induced running at m_a and use the pure SMEFT running below this scale. ALP contributions to the RG evolution of dimension-four parameters such as the top-quark Yukawa coupling y_t in (9) are found to be numerically irrelevant for the present analysis and have therefore been neglected.

The total χ^2 function is obtained by adding the individual contributions from low-energy observables, Higgs observables, and top data. The χ^2 functions for all these data sets, both written in terms of SMEFT Wilson coefficients and ALP parameters, are provided in the ancillary material.

3.2 Fit results

We present the limits on the ALP couplings at 95% CL and 99% CL in Figure 1. Assuming $f = 1$ TeV, we obtain $\mathcal{O}(1)$ bounds for C_{GG} , C_{WW} , C_{BB} and C_u , while C_d and C_e are much less

⁶Notice that the definition of C_{ll} and C_{ee} in these references differs by a factor 1/2 from the usual Warsaw basis definition. We have rescaled the corresponding Wilson coefficients to match the standard definitions employed for the Higgs and top sectors.

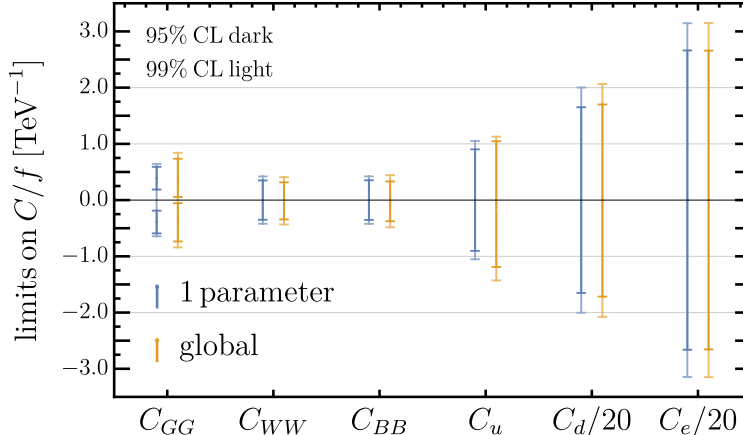


Figure 1: 95% CL (dark bars) and 99% CL limits (light bars) on the ALP couplings C/f evaluated at the scale $\Lambda = 4\pi f$ with $f = 1$ TeV. Bars in blue show the constraints obtained from individual one-parameter fits, while bars in orange refer to a global analysis marginalizing over the remaining parameters. The limits for C_d and C_e have been rescaled by a factor of $1/20$.

constrained, with limits of $\mathcal{O}(50)$. Our choice of the scale f is motivated by the hope that new physics beyond the SM exists at a scale $\Lambda = 4\pi f \approx 10$ TeV, as motivated by the hierarchy problem in light of current LHC results. Comparing the bounds from fitting one parameter at a time to those from a global analysis, we find that the limits on C_{WW} , C_{BB} , C_d , and C_e are minimally affected by the global analysis. Importantly, the weak constraints on C_d and C_e do not invalidate the limits imposed on the other Wilson coefficients in the global analysis. The global bounds on C_u and C_{GG} are weakened by 18% and 25% with respect to their one-parameter counterparts. For C_{GG} , we notice that the corresponding limit favors a non-zero value at 95% CL, but it is compatible with zero at 99% CL. This discrepancy is caused by a minor experimental anomaly in three highly correlated bins of the CMS simplified template cross section analysis in the $h \rightarrow ZZ$ channel [76], which favors non-zero values of C_{uH} or C_{uG} in the SMEFT and consequently shifts C_{GG} away from zero.

To investigate the correlations among the ALP couplings, we present two-dimensional fits in Figure 2. In each panel, we show the 95% CL bounds on two Wilson coefficients while setting the remaining coefficients to zero. As expected from the mild change of the global limits in Figure 1 with respect to the one-parameter fits, we find only weak correlations between most parameters. This is not surprising, since only few source terms of the SMEFT Wilson coefficients relevant for our analysis contain products of different ALP Wilson coefficients. Indeed, for the SMEFT Wilson coefficients appearing in our analysis, only C_{HWB} as well as the dipole operators $[C_{uG}]_{33}$, $[C_{uW}]_{33}$, $[C_{uB}]_{33}$ contain the products $C_{WW}C_{BB}$, and C_uC_{GG} , C_uC_{WW} , C_uC_{BB} , respectively, in the leading-logarithmic (LL) approximation. The most interesting correlation patterns are observed for the combinations $C_{GG}-C_u$ and $C_{WW}-C_{BB}$. For $C_{GG}-C_u$, a free-floating C_{GG} allows C_u to extend into a wider parameter region. The sign of the product of C_{GG} and C_u is however constrained to be negative at 95% CL when using the full data set. For C_{WW} and C_{BB} we find a slight preference for the product of the two coefficients to be positive.

It is interesting to study which of the considered data sets is the driving factor in constraining the individual Wilson coefficients. Individual bounds from low-energy, Higgs and top data sets are shown in Figure 2. Intriguingly, low-energy data dominate the constraints on C_{WW} , C_{BB} , C_e , and

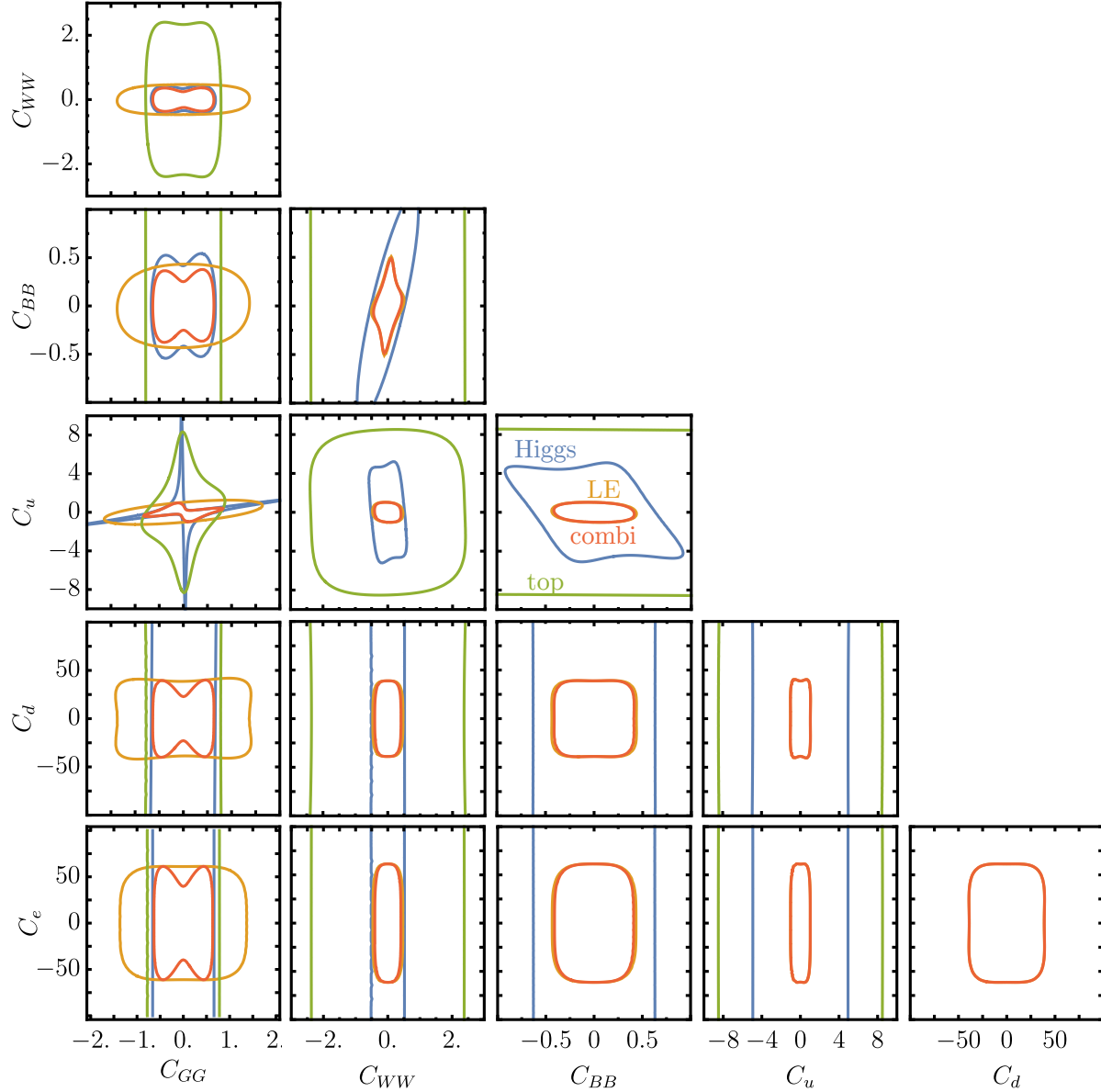


Figure 2: Two-dimensional 95% CL limits on the ALP couplings evaluated at the scale $\Lambda = 4\pi f$ with $f = 1$ TeV, where all other Wilson coefficients are set to zero in each panel. Different colors represent the limits from different experimental sources: low-energy (LE) data (orange), Higgs data (blue), and top data (green). The bounds derived from the combination of all experimental data are shown in red.

even C_u , which to first approximation describes the ALP–top coupling. As we discuss in the next subsection, the root of the strong constraint on C_u from low-energy data is that it mixes under RG evolution with C_{HD} , which is strongly constrained by the measurement of the W -boson mass. Only the bound on the ALP–gluon coupling C_{GG} receives important contributions from Higgs and top data. There is an interesting interplay between the bounds from different experiments for $C_{WW} - C_{BB}$ and $C_{GG} - C_u$. For $C_{WW} - C_{BB}$, Higgs data allow for a relatively wide parameter range as long as their product is positive. This degeneracy for C_{WW} and C_{BB} is broken by low-energy data. For the pair $C_{GG} - C_u$, top data slightly favor a positive product of C_{GG} and C_u , while Higgs data (as well as the combination of Higgs and top data) favor a negative product.

Leading-log approximation vs resummation

It is interesting to investigate how the bounds obtained from an exact solution in (12), in which the leading-logarithmic corrections are resummed to all orders, differ from those derived using the LL approximation truncated at one-loop order, which leads to the simple formula

$$C_i^{\text{SMEFT}}(\mu) \approx \gamma_{i\alpha\beta}^{\text{SMEFT-ALP}}(\Lambda) C_\alpha^{\text{ALP}}(\Lambda) [C_\beta^{\text{ALP}}(\Lambda)]^* \ln \frac{\mu}{\Lambda}. \quad (16)$$

For the low-energy observables at the Z pole, which dominate the fit for all coefficients except C_{GG} , a full list of LL parametrizations can be found in Appendix B. We show in Figure 3 the one-parameter limits on the ALP couplings obtained using the one-loop truncated LL approximation alongside with the constraints obtained from a full (resummed) evaluation of the scale evolution. For C_{WW} , C_{BB} , C_d , and C_e , the LL approximation captures the dominant effects and the limits only change marginally with respect to the resummed evolution. However, for C_{GG} and C_u the LL approximation lacks important effects. To investigate this further, we display the limits on C_u and C_{GG} from different experimental sources in the two rightmost panels of Figure 3. We observe that the limits on C_u from the top and Higgs sectors remain largely unchanged when using the LL approximation for the running. The main discrepancy arises from low-energy data, where the resummed running imposes tighter constraints than in the LL approximation. This discrepancy primarily originates from the RG evolution of the Wilson coefficient C_{HD} . While the ALP contribution from C_u to the Wilson coefficient C_{HD} vanishes at LL order, it is simple to see that this is not the case for the resummed result. The full RG equation for C_{HD} (neglecting for simplicity contributions proportional to $\alpha_i \neq \alpha_s$ and all Yukawa couplings except for y_t) reads [67,68]

$$\frac{d}{d \ln \mu} C_{HD} = \left(\frac{3\alpha_t}{\pi} + \frac{3\lambda}{8\pi^2} \right) C_{HD} + \frac{6\alpha_t}{\pi} [C_{Hq}^{(1)}]_{33} - \frac{6\alpha_t}{\pi} [C_{Hu}]_{33}, \quad (17)$$

with $\alpha_t \equiv y_t^2/(4\pi)$. The relevant ALP-induced terms that enter this RG equation are [43]

$$\frac{d}{d \ln \mu} [C_{Hq}^{(1)}]_{33} = -\pi \alpha_t C_u^2 + \dots, \quad \frac{d}{d \ln \mu} [C_{Hu}]_{33} = 2\pi \alpha_t C_u^2 + \dots, \quad (18)$$

where the ellipses refer to pure SMEFT contributions. Neglecting the running of the SM parameters results in the lowest-logarithmic approximation

$$C_{HD}(\mu) = -9\alpha_t^2 C_u^2 \ln^2 \frac{\mu}{\Lambda}, \quad (19)$$

which is a two-loop effect. Thus, bounds on C_{HD} only play a role in restricting the values of C_u beyond the strict LL approximation. Even though this is a subleading effect, strong bounds on C_{HD} from low-energy observables render it phenomenologically relevant for constraining C_u .

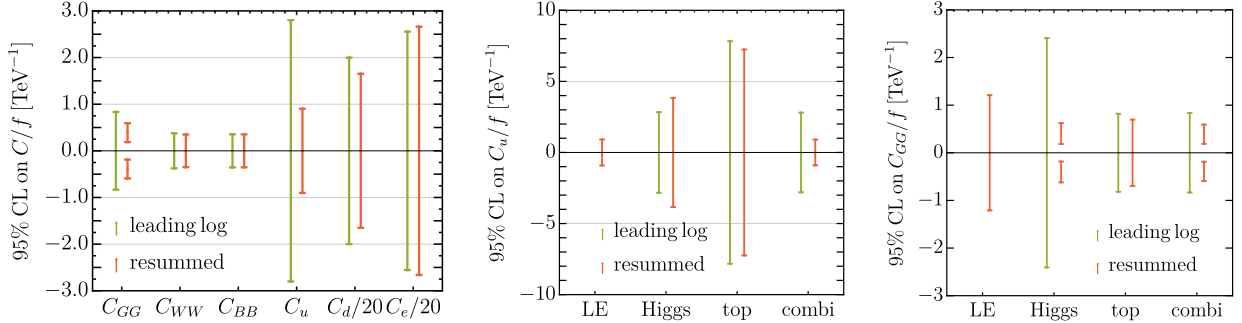


Figure 3: One-parameter fit limits on the ALP couplings using the one-loop truncated leading-logarithmic approximation (leading log) or the exact solution to the RG equations (resummed). The last two plots show the limits on C_u and C_{GG} derived from different experimental sources.

For C_{GG} , shown in the right-most panel of Figure 3, the LL approximation is able to reproduce the constraints originating from the top sector quite well. Limits from low-energy data vanish completely in the LL approximation, but this data set only plays a marginal role in constraining C_{GG} and hence does not influence the combined bounds. The dominant contribution to the combined constraints comes from Higgs data in this case. However, the LL approximation misses the most significant contributions from C_{HG} and $[C_{uG}]_{33}$ for this data set, which are tightly constrained through gluon-fusion Higgs production and are only sourced by C_{GG} beyond LL order. At lowest-logarithmic order, and taking into account the running of C_u [64], the solutions for C_{HG} , $[C_{uG}]_{33}$ in terms of C_{GG}^2 are given by

$$[C_{uG}]_{33}(\mu) \supset -\frac{25 g_s y_t \alpha_s}{\pi} C_{GG}^2 \ln^2 \frac{\mu}{\Lambda}, \quad C_{HG}(\mu) \supset \frac{100 \alpha_s^2 \alpha_t}{3} C_{GG}^2 \ln^3 \frac{\mu}{\Lambda}. \quad (20)$$

Both of the above estimates agree very well with the resummed results from the evolution tensor $U^{(5,5)}$ in (13).

Since most limits on the ALP couplings are well approximated at LL accuracy, we can deduce that they scale with the new-physics scale as $|C_i| \sim \Lambda \ln^{-1/2}(\Lambda/m_Z)$. As expected from the discussion above, the two exceptions to this scaling are C_u , for which we find $|C_u| \sim \Lambda \ln^{-1}(\Lambda/m_Z)$, and $C_{GG} \sim \Lambda \ln^n(\Lambda/m_Z)$ with $n = -3/2$ or $n = -1$, depending on whether $[C_{uG}]_{33}$ or C_{HG} dominates.

3.3 Comparison with bounds from direct searches

In this subsection, we compare our indirect limits to direct limits on ALP couplings obtained in the literature. Since direct bounds are typically stronger for light ALPs, we focus on $\mathcal{O}(\text{GeV})$ ALP masses, where we expect our indirect, (mostly) mass-independent limits to be more competitive. Direct limits in this regime are dominated by collider [31] and flavor [38] experiments.⁷ We compare the direct and indirect bounds on the ALP Wilson coefficients in Figure 4, where the indirect bounds obtained from our global analysis are shown in red. The most relevant direct constraints on each of the individual ALP couplings are the following:

- **C_{GG} :** Flavor data impose the strongest direct constraints across the majority of the depicted ALP mass range. However, around $m_a \sim 100$ GeV, the inclusion of LHC multijet constraints becomes crucial [77].

⁷The results in [38] are given in terms of the Wilson coefficients in (2). Therefore, a translation between their notation and ours is needed to compare the constraints, leading to apparent weaker limits in some cases.

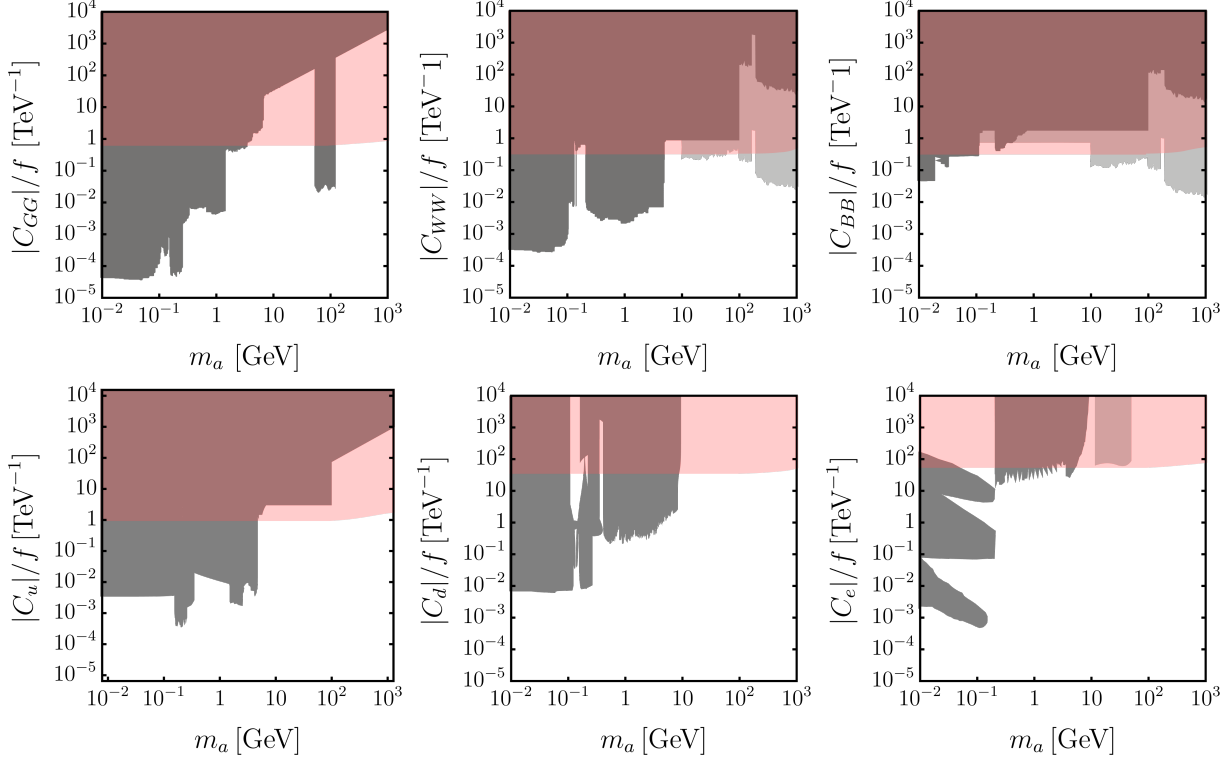


Figure 4: Indirect 95% CL limits from ALP–SMEFT interference (red) compared to direct bounds from flavor, beam dump, and collider experiments, as well as supernova data. All direct bounds assume the remaining ALP Wilson coefficients to be zero. Direct bounds shaded in light gray are subject to additional model assumptions, see text for details. Note that we do not show the lower bound on C_{GG} , excluding a non-zero value at 95% CL, as this bound disappears at 99% CL.

- **C_{WW} and C_{BB} :** In addition to flavor constraints, non-resonant ALP contributions to vector-boson scattering yield mass-independent direct bounds on ALPs with masses up to ~ 100 GeV [78]. For non-resonant gluon-fusion ALP production followed by its decay to gauge bosons [79–81], constraints are placed on the products of the ALP–gluon coupling with the ALP–photon, $C_{\gamma\gamma} = s_W^2 C_{WW} + c_W^2 C_{BB}$, or the ALP–Z, $C_{ZZ} = c_W^2 C_{WW} + s_W^2 C_{BB}$, couplings.⁸ Specifically, $|C_{ZZ} C_{GG}|/f^2 < 4 \cdot 10^{-2} \text{ TeV}^{-2}$ [81] and $|C_{\gamma\gamma} C_{GG}|/f^2 < 5 \cdot 10^{-3} \text{ TeV}^{-2}$ [79]. As these bounds involve products of ALP parameters, they are not shown in our plots which depict the bounds for one coupling at a time. However, we point out that they provide the dominant bounds in the limit in which both Wilson coefficients are sizable. In the high ALP-mass region, we present bounds derived from collider constraints on the ALP–photon coupling [32]. The corresponding limits are shown in light gray to highlight their model dependence. It is important to note that for heavy ALPs with $m_a > m_Z$, where additional decay channels like $a \rightarrow Z\gamma$ open up, a dominant decay to photons becomes highly unlikely [82]. In darker gray, we present the same limits assuming a branching ratio into photons of 10^{-3} .
- **C_u and C_d :** Constraints on the ALP parameter space stem from flavor data that, for the case of C_u , cover the full displayed ALP-mass range. In addition, C_u gets further constrained by LHC $t\bar{t}$ searches for $m_a \leq 100$ GeV [83].

⁸Here, c_W (s_W) is the cosine (sine) of the weak-mixing angle.

- C_e : We present direct bounds from flavor and dark photon searches at BaBar [84], which cover a similar mass range compared to constraints from Υ decays. Furthermore, we include constraints from SN1987A supernova observations [85] and beam dump searches at SLAC [86], which are relevant in the $m_a < 1$ GeV mass range. In the 11.5 – 50 GeV mass range, we consider LHC constraints on $h \rightarrow a\mu\bar{\mu}$ [87], assuming a 100% branching ratio of the ALP to muons. These constraints are shaded in a lighter gray to account for the possibility of decays to taus, which would weaken the bounds.

Overall, we find that the ALP – SMEFT interference can constraint previously untested regions of the ALP parameter space. Furthermore, most direct bounds have specific model assumptions, often requiring all remaining coefficients to be zero, that do not apply to our indirect bounds. The indirect limits presented here thus offer good complementary probes, even in cases where the direct limits would a priori seem more competitive.

4 Interpretation in terms of UV-complete models

We now reinterpret our bounds in terms of UV-complete ALP models. In particular, we describe the effect of including SMEFT contributions beyond the RG-induced effects considered before, which stem from the incorporation of (tree-level) threshold corrections. We focus in the two main (fundamental) axion UV completions: the Kim-Shifman-Vainshtein-Zakharov (KSVZ) [39, 40] and the Dine-Fischler-Srednicki-Zhitnitsky (DFSZ) [41, 42] models, which have been already proposed as ALP benchmark scenarios [88].

4.1 KSVZ model

The KSVZ model extends the SM with a pair of fermions, Q_L and Q_R , which transform non-trivially under $SU(3)_c$ and chirally under a global $U(1)_A$ symmetry, and a SM-singlet scalar S , which is only charged under the $U(1)_A$ symmetry and acquires a non-zero vacuum expectation value (vev), thus spontaneously breaking the global symmetry. The most general Lagrangian for this model reads

$$\begin{aligned} \mathcal{L}_{\text{KSVZ}} = & \mathcal{L}_{\text{SM}} + |\partial_\mu S|^2 + \bar{Q} i \not{D} Q - y_Q (S \bar{Q}_L Q_R + \text{h.c.}) \\ & + \mu_S^2 |S|^2 - \frac{\lambda_S}{2} |S|^4 - \lambda_{SH} |S|^2 (H^\dagger H) + \mathcal{L}_{Qq}, \end{aligned} \quad (21)$$

where y_Q , μ_S , λ_S , and λ_{SH} are real parameters and \mathcal{L}_{Qq} is a possible portal coupling between Q and a SM fermion. As discussed in [89], this term is introduced to let the extra quarks decay, as otherwise the Lagrangian would be invariant under a vectorial $U(1)_Q$ symmetry that would make them stable. In the original KSVZ implementation, where the extra quarks transform under the SM as $Q_{L,R} \sim (\mathbf{3}, \mathbf{1})_0$, no renormalizable term for \mathcal{L}_{Qq} is possible. However, there are multiple representation choices for which $\mathcal{L}_{Qq} \neq 0$. For concreteness, we consider here the case where $Q_{L,R} \sim (\mathbf{3}, \mathbf{1})_{-1/3}$ and the global $U(1)_A$ charges are $X_S = 1$, $X_{Q_L} = 1$, and $X_{Q_R} = 0$. In this case, we have

$$\mathcal{L}_{Qq} = -y_q^p \bar{q}_L^p H Q_R + \text{h.c.} \quad (22)$$

Additionally, we consider possible soft $U(1)_A$ -breaking terms that will give mass to the pseudo-Goldstone ALP at the expense of spoiling the solution to the strong CP problem. For definiteness, we consider the term

$$\mathcal{L} = \mathcal{L}_{\text{KSVZ}} + \frac{\kappa^2}{2} (S^2 + S^{*2}), \quad (23)$$

with κ being a real parameter controlling the size of the breaking.

In the $U(1)_A$ -broken phase, it is convenient to write the scalar singlet as

$$S(x) = \frac{1}{\sqrt{2}} [f + \rho(x)] e^{\frac{ia(x)}{f}}, \quad (24)$$

with f denoting the vev of S , and ρ and a corresponding to the radial and pseudo-Goldstone components of the field, respectively. After performing the fermion shift

$$Q_L \rightarrow e^{\frac{ia}{f}} Q_L, \quad (25)$$

which removes the ALP from the Yukawa interaction, the UV Lagrangian in the $U(1)_A$ -broken phase reads

$$\begin{aligned} \mathcal{L} = & \mathcal{L}_{\text{SM}} - \frac{\lambda_{SH} f^2}{2} (H^\dagger H) + \frac{1}{2} (\partial_\mu \rho)^2 + \frac{1}{2} \left(1 + \frac{\rho}{f}\right)^2 (\partial_\mu a)^2 + \bar{Q} i \not{D} Q - \frac{\partial_\mu a}{f} \bar{Q}_L \gamma^\mu Q_L \\ & - \frac{a}{f} \frac{\alpha_s}{8\pi} G_{\mu\nu}^A \tilde{G}^{\mu\nu A} - \frac{1}{3} \frac{a}{f} \frac{\alpha_Y}{4\pi} B_{\mu\nu} \tilde{B}^{\mu\nu} - \left[M_Q \left(1 + \frac{\rho}{f}\right) \bar{Q}_L Q_R + y_q^p \bar{q}_L^p H Q_R + \text{h.c.} \right] \\ & - \frac{1}{2} M_\rho^2 \rho^2 - 3\lambda_S f \frac{\rho^3}{3!} - 3\lambda_S \frac{\rho^4}{4!} - \lambda_{SH} \left(f \rho + \frac{\rho^2}{2} \right) (H^\dagger H) - \frac{m_a^2}{4} (f + \rho)^2 \left(1 - \cos \frac{2a}{f} \right), \quad (26) \end{aligned}$$

with $M_Q = y_Q f / \sqrt{2}$, $M_\rho^2 = \lambda_S f^2$ and $m_a^2 = 2\kappa^2$. Note that, after $U(1)_A$ -symmetry breaking, the Higgs doublet mass gets a correction of order $\lambda_{SH} f$. Thus, if the hierarchy between the electroweak scale and f is large, one would expect $\lambda_{SH} \sim v^2 / f^2$ to avoid a fine-tuned cancellation of parameters.

We consider the scenario in which $M_\rho, M_Q \sim f$ are heavy and integrate out the corresponding particles. The resulting EFT Lagrangian at tree-level order and up to dimension-six interactions reads⁹

$$\begin{aligned} \mathcal{L}_{\text{EFT}} = & \mathcal{L}_{\text{SM}} - \frac{\lambda_{SH} f^2}{2} (H^\dagger H) + \frac{1}{2} \frac{f^2 \lambda_{SH}^2}{M_\rho^2} (H^\dagger H)^2 + \frac{1}{2} (\partial_\mu a)^2 - \frac{1}{2} m_a^2 a^2 - \frac{a}{f} \frac{\alpha_s}{8\pi} G_{\mu\nu}^A \tilde{G}^{\mu\nu A} \\ & - \frac{1}{3} \frac{a}{f} \frac{\alpha_Y}{4\pi} B_{\mu\nu} \tilde{B}^{\mu\nu} + 4 \frac{m_a^2}{f^2} \frac{a^4}{4!} + \lambda_{SH} \frac{m_a^2}{M_\rho^2} a^2 (H^\dagger H) - \frac{\lambda_{SH}}{M_\rho^2} (\partial_\mu a)^2 (H^\dagger H) \\ & - \frac{\lambda_{SH}^2 f^2}{2M_\rho^4} Q_{H\Box} + \frac{y_q^p y_q^{r*}}{2M_Q^2} \left(\mathbf{Y}_d^{rs} [Q_{dH}]^{ps} - \frac{1}{2} [Q_{Hq}^{(1)}]^{pr} - \frac{1}{2} [Q_{Hq}^{(3)}]^{pr} + \text{h.c.} \right), \quad (27) \end{aligned}$$

where the second and third terms are removed by an appropriate redefinition of the Higgs potential parameters. Namely,

$$\mu^2 \rightarrow \tilde{\mu}^2 = \mu^2 - \frac{\lambda_{SH} f^2}{2}, \quad \lambda \rightarrow \tilde{\lambda} = \lambda - \frac{f^2 \lambda_{SH}^2}{2M_\rho^2}. \quad (28)$$

Furthermore, we see that the explicit $U(1)_A$ -breaking term not only gives mass to the ALP, but also introduces other shift-symmetry breaking interactions, $m_a^2 a^4$ and $m_a^2 a^2 (H^\dagger H)$.¹⁰ Finally, Q_i are dimension-six SMEFT operators whose definition can be found in [63].

We now turn to analyzing constraints on the KSVZ model from Higgs, top and low-energy data. As discussed above, the KSVZ model features a fermiophobic axion (at tree-level order),

⁹We have used the `Mathematica` package `Matchete` [90] to cross-check this matching result.

¹⁰These additional shift-symmetry breaking interactions do not alter our results in Sections 2 and 3, except for the running of m_H in (9), which receives similar effects to those from c_{HH} .

with different Q charges under the SM gauge group yielding different values C_{GG} , C_{WW} and C_{BB} . A common feature of all KSVZ models is the presence of a non-zero $Q_{H\Box}$, which is generated via the tree-level exchange of the associated scalar radial excitation. Profiling over the remaining parameters, we obtain the constraint $\lambda_S^2 f/\lambda_{SH} > 2.8 \text{ TeV}$ from the limits on the $Q_{H\Box}$ coefficient. On the other hand, the limits on the bosonic ALP couplings when profiling over the remaining parameters (including the Wilson coefficient of $Q_{H\Box}$) do not change by more than 10% with respect to the one-parameter limits presented in Figure 1. Therefore, we refer to this plot for limits on KSVZ models with generic Q charges.

For KSVZ models with additional portal couplings for the heavy vector-like quarks, such as the one presented in (27), we can additionally set constraints on the coupling strength of the portal coupling y_q . Assuming for simplicity that y_q is flavor universal, we find the limit $|y_q/M_Q| < 0.1 \text{ TeV}^{-1}$, which is dominated by the strong constraints on $C_{Hq}^{(1)}$ and $C_{Hq}^{(3)}$ from electroweak precision observables.

4.2 DFSZ model

The DFSZ models consists of a two-Higgs-doublet, $H_{1,2}$, plus SM-singlet, S , scalar extension of the SM. The Lagrangian of the model is chosen such that it preserves, at the classical level, a global $U(1)_A$ symmetry and reads

$$\begin{aligned} \mathcal{L}_{\text{DFSZ}} \supset & |D_\mu H_1|^2 + |D_\mu H_2|^2 + |\partial_\mu S|^2 - (\bar{q} \tilde{H}_1 \mathbf{\Gamma}_u u_R + \bar{q} H_2 \mathbf{\Gamma}_d d_R + \bar{\ell} H_i \mathbf{\Gamma}_e e_R + \text{h.c.}) \\ & - m_1^2 |H_1|^2 - m_2^2 |H_2|^2 - \frac{\lambda_1}{2} |H_1|^4 - \frac{\lambda_2}{2} |H_2|^4 - \lambda_3 |H_1|^2 |H_2|^2 - \lambda_4 |H_1^\dagger H_2|^2 \\ & + \mu_S^2 |S|^2 - \frac{\lambda_S}{2} |S|^4 - \lambda_{SH_1} |S|^2 |H_1|^2 - \lambda_{SH_2} |S|^2 |H_2|^2 - \lambda_{SH_{12}} \left[(H_1^\dagger H_2) S^2 + \text{h.c.} \right], \end{aligned} \quad (29)$$

where \supset denotes that we omitted the SM-like terms in the Lagrangian. All scalar potential parameters in the Lagrangian above are real, including $\lambda_{SH_{12}}$ which can be made real by appropriate global phase redefinitions of the fields. In the charged-lepton Yukawa, $i = 1, 2$ corresponds to two different versions of the model, which we denote as DFSZ I and II, respectively. The last term also admits a different choice, with S rather than S^2 , corresponding to a different $U(1)_A$ charge implementation. Different choices for this term have mild effects in the ensuing discussion and we focus on this variant of the model for definiteness. As we did for the KSVZ model, we admit the possibility of an explicit $U(1)_A$ -breaking term, which we choose to be the same as before

$$\mathcal{L} = \mathcal{L}_{\text{DFSZ}} + \frac{\kappa^2}{2} (S^2 + S^{*2}), \quad (30)$$

with κ being a real parameter controlling the size of the breaking.

As before, the scalar potential parameters are chosen such that S acquires a vev that breaks the global $U(1)_A$ symmetry. Once more, we parameterize the SM-singlet as

$$S(x) = \frac{1}{\sqrt{2}} [f + \rho(x)] e^{\frac{ia(x)}{f}}. \quad (31)$$

The two-Higgs-doublet spectrum can be rather different depending on the values of m_1 , m_2 and λ_{SH_i} . Here, we assume that these parameters are such that we are in a decoupling regime where a full doublet and ρ are much heavier than the ALP and the SM particles.¹¹ The heavy doublet, Φ ,

¹¹It would be interesting to consider a low-scale two-Higgs-doublet regime, see e.g. [91, 92], where we depart from our original assumption that the ALP-SMEFT Lagrangian in (1) is the relevant EFT. This would require extending the present EFT framework and is beyond the scope of this work.

and SM Higgs, H , are linear combinations of H_1 and H_2 . Namely,

$$\begin{pmatrix} H_1 \\ H_2 \end{pmatrix} = R(\alpha) \begin{pmatrix} H \\ \Phi \end{pmatrix} \quad \text{such that} \quad R(\alpha)^T \begin{pmatrix} m_{11}^2 & m_{12}^2 \\ m_{12}^2 & m_{22}^2 \end{pmatrix} R(\alpha) = \begin{pmatrix} -\mu^2 & 0 \\ 0 & M_\Phi^2 \end{pmatrix}, \quad (32)$$

where $m_{ii}^2 = m_i^2 + \lambda_{SH_i} f^2/2$ ($i = 1, 2$), $m_{12}^2 = \lambda_{SH_{12}} f^2/2$, and $R(\alpha)$ is a 2×2 rotation matrix. Once this rotation is taken into account, the SM Yukawas are related to the mixing angle and the original Yukawas as

$$\mathbf{Y}_u = c_\alpha \mathbf{\Gamma}_u, \quad \mathbf{Y}_d = s_\alpha \mathbf{\Gamma}_d, \quad \mathbf{Y}_e = \begin{cases} c_\alpha \mathbf{\Gamma}_e & \text{DFSZ I} \\ s_\alpha \mathbf{\Gamma}_e & \text{DFSZ II} \end{cases}, \quad (33)$$

with $c_\alpha \equiv \cos \alpha$, and $s_\alpha \equiv \sin \alpha$. Perturbativity constraints on the UV Yukawa couplings restrict the possible values of α . Using the perturbative unitarity bound $|\Gamma_u^{33}| \lesssim 3$ [93], we get the constraints $|c_\alpha| \gtrsim y_t/3$ and $|s_\alpha| \gtrsim y_b/3$, independently of the DFSZ type.

The pseudo-Goldstone, a , can be moved away from the scalar potential, yielding a coupling structure like the one in (2), by means of the following shifts of the scalar and fermion fields

$$\begin{aligned} H_1 &\rightarrow e^{\frac{ia}{f} X_{H_1}} H_1, & H_2 &\rightarrow e^{\frac{ia}{f} X_{H_2}} H_2, \\ u_R &\rightarrow e^{\frac{ia}{f} X_{H_1}} u_R, & d_R &\rightarrow e^{-\frac{ia}{f} X_{H_2}} d_R, & e_R &\rightarrow e^{-\frac{ia}{f} X_{H_i}} e_R, \end{aligned} \quad (34)$$

with $X_{H_1} = 2s_\alpha^2$ and $X_{H_2} = -2c_\alpha^2$.¹² After performing these shifts and the Higgs rotation in (32), we obtain the following UV Lagrangian in the $U(1)_A$ -broken phase

$$\begin{aligned} \mathcal{L} \supset \mathcal{L}_{\text{SM}} &+ \left[\frac{1}{2} \left(1 + \frac{\rho}{f} \right)^2 + s_{2\alpha}^2 \frac{|H|^2}{f^2} \right] (\partial_\mu a)^2 + c_u \frac{\partial_\mu a}{f} \bar{u}_R \gamma^\mu u_R + c_d \frac{\partial_\mu a}{f} \bar{d}_R \gamma^\mu d_R + c_e \frac{\partial_\mu a}{f} \bar{e}_R \gamma^\mu e_R \\ &+ 3 \frac{a}{f} \frac{\alpha_s}{4\pi} G_{\mu\nu}^A \tilde{G}^{\mu\nu A} + c_{BB} \frac{a}{f} \frac{\alpha_Y}{4\pi} B_{\mu\nu} \tilde{B}^{\mu\nu} + |D_\mu \Phi|^2 - M_\Phi |\Phi|^2 + \frac{1}{2} (\partial_\mu \rho)^2 - \frac{1}{2} M_\rho^2 \rho^2 \\ &- \left[-t_\alpha \bar{q} \tilde{\Phi} \mathbf{Y}_u u_R + t_\alpha^{-1} \bar{q} \tilde{\Phi} \mathbf{Y}_d d_R + \eta_\alpha \bar{\ell} \Phi \mathbf{Y}_e e_R + \lambda_{\Phi H} |H|^2 (H^\dagger \Phi) + \lambda_{S\Phi H} f \rho (H^\dagger \Phi) + \text{h.c.} \right] \\ &- 3\lambda_S f \frac{\rho^3}{3!} - 3\lambda_S \frac{\rho^4}{4!} - \frac{m_a^2}{4} (f + \rho)^2 \left(1 - \cos \frac{2a}{f} \right) - \lambda_{SH} \left(f\rho + \frac{\rho^2}{2} \right) |H|^2, \end{aligned} \quad (35)$$

where $M_\rho^2 = \lambda_S f^2$, $m_a^2 = 2\kappa^2$, $t_\alpha \equiv \tan \alpha$ and $\eta_\alpha = -t_\alpha (t_\alpha^{-1})$ for DFSZ I (II), and we omitted the Lagrangian terms involving heavy fields (either Φ or ρ) that do not contribute to the tree-level matching at dimension six. The dimension-five ALP couplings depend on the model variant and are given by $c_u = -c_e = -2s_\alpha^2$, $c_d = -2c_\alpha^2$, $c_{BB} = 2$ in DFSZ I, while $c_u = -2s_\alpha^2$, $c_d = c_e = -2c_\alpha^2$, $c_{BB} = 8$ in DFSZ II. Finally, we have defined the following couplings for simplicity

$$\begin{aligned} \lambda_{\Phi H} &= s_\alpha c_\alpha [-c_\alpha^2 \lambda_1 + s_\alpha^2 \lambda_2 + c_{2\alpha} (\lambda_3 + \lambda_4)], & \lambda_{SH} &= s_{2\alpha} \lambda_{SH_{12}} + c_\alpha^2 \lambda_{SH_1} + s_\alpha^2 \lambda_{SH_2}, \\ \lambda_{S\Phi H} &= \frac{1}{2} [2c_{2\alpha} \lambda_{SH_{12}} - s_{2\alpha} (\lambda_{SH_1} - \lambda_{SH_2})]. \end{aligned} \quad (36)$$

We integrate out the ρ and Φ fields at tree-level with the help of **Matchete** [90]. The resulting EFT Lagrangian at dimension-six reads

$$\mathcal{L}_{\text{EFT}} = \mathcal{L}_{\text{SM}} + \frac{1}{2} (\partial_\mu a)^2 - \frac{1}{2} m_a^2 a^2 + 3 \frac{a}{f} \frac{\alpha_s}{4\pi} G_{\mu\nu}^A \tilde{G}^{\mu\nu A} + c_{BB} \frac{a}{f} \frac{\alpha_Y}{4\pi} B_{\mu\nu} \tilde{B}^{\mu\nu} + c_u \frac{\partial_\mu a}{f} \bar{u}_R \gamma^\mu u_R$$

¹²This choice of $H_{1,2}$ shifts is uniquely determined by the requirement of having no contributions to the $\partial^\mu a (H^\dagger i \overleftrightarrow{D}_\mu H)$ operator, which would introduce a mixing between the ALP and the Z would-be Goldstone boson after electroweak symmetry breaking.

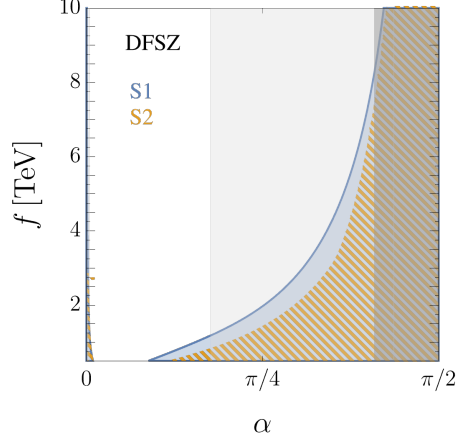


Figure 5: Two-dimensional limits on α vs f in the DFSZ model for two benchmark scenarios: S1 (benchmark) and S2 (profiled), see text for details. The dark and light gray bands corresponds to regions where perturbative unitarity is violated (namely, $\Gamma_u^{33} \gtrsim 3$) and where $\Gamma_u^{33} \gtrsim 1$, respectively.

$$\begin{aligned}
& + c_d \frac{\partial_{\mu} a}{f} \bar{d}_R \gamma^{\mu} d_R + c_e \frac{\partial_{\mu} a}{f} \bar{e}_R \gamma^{\mu} e_R + 4 \frac{m_a^2}{f^2} \frac{a^4}{4!} - \left(\frac{\lambda_{SH}}{M_{\rho}^2} - \frac{s_{2\alpha}^2}{f^2} \right) (\partial_{\mu} a)^2 |H|^2 \\
& + \lambda_{SH} \frac{m_a^2}{M_{\rho}^2} a^2 |H|^2 - \frac{C_{\psi H}}{M_{\Phi}^2} (t_{\alpha} [\mathbf{Y}_u]^{pr} [Q_{uH}]^{pr} - t_{\alpha}^{-1} [\mathbf{Y}_d]^{pr} [Q_{dH}]^{pr} - \eta_{\alpha} [\mathbf{Y}_e]^{pr} [Q_{eH}]^{pr} + \text{h.c.}) \\
& - \frac{[\mathbf{Y}_u^*]^{sr} [\mathbf{Y}_u]^{pt} t_{\alpha}^2}{M_{\Phi}^2} \left(\frac{1}{6} [Q_{qu}^{(1)}]^{prst} + [Q_{qu}^{(8)}]^{prst} \right) - \frac{[\mathbf{Y}_d^*]^{sr} [\mathbf{Y}_d]^{pt} t_{\alpha}^{-2}}{M_{\Phi}^2} \left(\frac{1}{6} [Q_{qd}^{(1)}]^{prst} + [Q_{qd}^{(8)}]^{prst} \right) \\
& - \frac{[\mathbf{Y}_e^*]^{sr} [\mathbf{Y}_e]^{pt} \eta_{\alpha}^2}{2M_{\Phi}^2} [Q_{le}]^{prst} - \frac{1}{M_{\Phi}^2} \left([\mathbf{Y}_u]^{pr} [\mathbf{Y}_d]^{st} [Q_{quqd}^{(1)}]^{prst} - [\mathbf{Y}_u]^{st} [\mathbf{Y}_e]^{pr} t_{\alpha} \eta_{\alpha} [Q_{lequ}^{(1)}]^{prst} \right. \\
& \left. - [\mathbf{Y}_d^*]^{st} [\mathbf{Y}_e]^{pr} t_{\alpha}^{-1} \eta_{\alpha} [Q_{ledq}]^{prst} + \text{h.c.} \right) + \frac{C_H}{M_{\Phi}^2} Q_H - \frac{\lambda_{SH}^2 f^2}{2M_{\rho}^4} Q_{H\Box}, \tag{37}
\end{aligned}$$

where $C_{\psi H}$ and C_H are given in terms of the original scalar-potential parameters by

$$C_H = C_{\psi H}^2, \quad C_{\psi H} = \lambda_{\Phi H} - \lambda_{SH} \lambda_{S\Phi H} \frac{f^2}{M_{\rho}^2}. \tag{38}$$

Analogously to what we did in the KSVZ case, we have redefined the SM Higgs potential parameters, μ and λ , to account for the matching corrections. If the hierarchy between the electroweak scale and f is large, one would again expect $\lambda_{SH} \sim v^2/f^2$ to avoid a fine-tuned cancellation of scalar-potential parameters.

Translating the above notation to the one used in our global analysis (cf. (4)), we find that only ALP couplings to fermions are non-zero in both DFSZ models: $C_u = -C_e = -2s_{\alpha}^2$ and $C_d = -2c_{\alpha}^2$ for DFSZ I, and $C_u = -2s_{\alpha}^2$ and $C_d = C_e = -2c_{\alpha}^2$ for DFSZ II. We present the bounds on the mixing angle α and the ALP decay constant f in Figure 5. We consider two scenarios: S1) where the coefficients of the SMEFT operators Q_H , $Q_{H\Box}$, and $Q_{\psi H}$ are assumed to be suppressed, as would be expected if the scalar-potential parameters are small; and S2) where we profile over the coefficients of these operators within the range $|C_{\psi H}|, |C_{H\Box}|, |C_H| < 1$. Since the ALP couplings to fermions in the DFSZ I and DFSZ II models differ only by their couplings to leptons, which are weakly constrained, we find that the limits on both models are (almost) identical. As shown

in Figure 5, the overall limit on f is dominated by the matching correction from the four-quark operators $Q_{qu}^{(8)}$ and in particular $Q_{qu}^{(1)}$, which run into the coefficients of the SMEFT operators Q_{HD} , $Q_{Hq}^{(1)}$ and $Q_{Hq}^{(3)}$ that are tightly constrained at the electroweak scale. The obtained limits are found to be weak, except in the region where the UV Yukawa couplings are larger than one and dominates close to the non-perturbative Yukawa region. Limits from the ALP coupling to up-type quarks are suppressed by s_α^2 and thus only play a subdominant role. When profiling over the other matching corrections within the range $|C_{\psi H}|, |C_{H\Box}|, |C_H| < 1$, we observe that the limits on both DFSZ models are slightly diminished with respect to S1, especially for intermediate values of $|\alpha|$.

5 Conclusions

While the SMEFT is normally used to describe the possible effects of yet undiscovered heavy particles, we have shown in this paper that SMEFT analyses can also be reinterpreted to infer indirect information on light new physics. Exploiting the non-trivial RG flow of the ALP couplings into the SMEFT Wilson coefficients [43], we have used existing SMEFT studies including low-energy, Higgs and top data to constrain these couplings. Contrary to other ALP constraints, the ones presented here possess the unique feature of being largely independent of particular assumptions on the ALP mass, lifetime or branching ratios.

Furthermore, we have obtained for the first time, a semi-analytic solution to the ALP RG equations at dimension six under the assumption of flavor-universal ALP interactions. This solution, given in the form of RG evolution tensors, can readily be used to derive ALP and SMEFT couplings at an arbitrary scale (provided there are no mass thresholds). Its generalization to generic ALP interactions and the incorporation of threshold corrections into a modified version of `DsixTools` will be presented in a forthcoming publication, thus paving the way for automated ALP analyses. Even with the present assumptions, the ALP-to-SMEFT evolution tensor provided in the ancillary files can readily be used in most SMEFT analyses, such as the one presented in this paper.

The resulting bounds on the bosonic ALP interactions C_{GG} , C_{WW} , C_{BB} and the ALP coupling to up-type quarks C_u are found to be of $\mathcal{O}(1)$ for $f = 1$ TeV. The couplings to down-type quarks and leptons, C_d and C_e , remain weakly constrained, with limits of $\mathcal{O}(50)$, as expected given the additional Yukawa suppression present in these couplings. The bounds on C_{WW} , C_{BB} , C_u , C_d , and C_e primarily arise from low-energy precision observables, such as measurements at the Z pole. On the contrary, the limit on C_{GG} is mainly driven by Higgs and top physics. In our global analysis, we found weak correlations between Wilson coefficients. However, there is an interesting interplay between the limits on C_u and C_{GG} , where a negative product of the two Wilson coefficients is favored, and on C_{WW} and C_{BB} , where any large product of the two coefficients is ruled out. We have also found that the LL approximation captures most of the phenomenologically-relevant effects for all ALP couplings except C_u and C_{GG} , which generate non-trivial contributions to strongly constrained SMEFT directions at higher order in the RG resummation.

Comparing with direct ALP searches, our limits constrain large regions of previously uncovered areas of the parameter space for ALP masses above 10 GeV. Even for lower masses, the obtained bounds can partly compete with existing ones and have the major advantage of being independent of specific assumptions on the ALP properties, thus offering a complementary probe in regions where direct bounds would a priori dominate. It would be interesting to investigate how the combination of direct and indirect bounds further narrows the ALP parameter space in a global analysis. We leave the comprehensive study of both direct and indirect constraints in a global analysis for future work.

We have also reinterpreted our results in the context of two benchmark UV completions based on the KSVZ and DSFZ models. The KSVZ model features no tree-level couplings to fermions and we have found that tree-level threshold corrections, arising from integrating out additional heavy particles present in the model, do not significantly affect the limits on C_{GG} , C_{WW} and C_{BB} obtained from the ALP–SMEFT analysis. On the contrary, the DSFZ models we studied yield only fermionic ALP couplings. In this case, we found that tree-level threshold corrections can be more important and dominate the model constraints. However, the model remains weakly constrained except in regions where the UV Yukawas are large. A more dedicated study including different assumptions on the mass spectrum, additional observables or incorporating one-loop threshold corrections remains to be explored in future studies.

Acknowledgments

We thank Martín González Alonso for sharing the χ^2 of the global fit in [60], and the authors of [38] for providing us with a `Mathematica` version of their results. A.B. gratefully acknowledges support from the Alexander-von-Humboldt foundation as a Feodor Lynen Fellow. J.F.M. thanks the Theoretical High Energy Physics Department at JGU Mainz for hospitality and support during his stay as a visitor. The work of J.F.M. is supported by the Spanish Ministry of Science and Innovation (MCIN) and the European Union NextGenerationEU/PRTR under grant IJC2020-043549-I, by the MCIN and State Research Agency (SRA) projects PID2019-106087GB-C22 and PID2022-139466NB-C21 (ERDF), and by the Junta de Andalucía projects P21_00199 and FQM101. The research of A.M.G. and M.N. was supported by the Cluster of Excellence *Precision Physics, Fundamental Interactions and Structure of Matter* (PRISMA⁺ – EXC 2118/1) within the German Excellence Strategy (project ID 39083149).

A Experimental inputs

The experimental observables included in our fit from the Higgs and top sectors are summarized in Tables 1–3.

Table 1: Higgs observables included in the fit.

Observables		no. of measurements	References
Higgs Data		154	
7 and 8 TeV Run-I data	ATLAS & CMS combination	20	Table 8 of [94]
	ATLAS & CMS combination $\mu(h \rightarrow \mu\mu)$	1	Table 13 of [94]
	ATLAS $\mu(h \rightarrow Z\gamma)$	1	Figure 1 of [95]
13 TeV ATLAS Run-II data	$\mu(h \rightarrow Z\gamma)$ at 139 fb ⁻¹	1	[96]
	$\mu(h \rightarrow \mu\mu)$ at 139 fb ⁻¹	1	[97]
	$\mu(h \rightarrow \tau\tau)$ at 139 fb ⁻¹	4	Figure 14 of [98]
	$\mu(h \rightarrow bb)$ in VBF and ttH at 139 fb ⁻¹	1+1	[99,100]
	STXS $h \rightarrow \gamma\gamma/ZZ/b\bar{b}$ at 139 fb ⁻¹	42	Figures 1 and 2 of [74]
	STXS $h \rightarrow WW$ in ggF, VBF at 139 fb ⁻¹	11	Figures 12 and 14 of [101]
13 TeV CMS Run-II data	$\mu(h \rightarrow b\bar{b})$ in Vh at 35.9/41.5 fb ⁻¹	2	entries from Table 4 of [102]
	$\mu(h \rightarrow WW)$ in ggF at 137 fb ⁻¹	1	[103]
	$\mu(h \rightarrow \mu\mu)$ at 137 fb ⁻¹	4	Figure 11 of [104]
	$\mu(h \rightarrow \tau\tau/WW)$ in $t\bar{t}h$ at 137 fb ⁻¹	3	Figure 14 of [105]
	STXS $h \rightarrow WW$ at 137 fb ⁻¹ in Vh	4	Table 9 of [106]
	STXS $h \rightarrow \tau\tau$ at 137 fb ⁻¹	11	Figures 11 and 12 of [107]
	STXS $h \rightarrow \gamma\gamma$ at 137 fb ⁻¹	27	Table 13 and Figure 21 of [108]
	STXS $h \rightarrow ZZ$ at 137 fb ⁻¹	18	Table 6 and Figure 15 of [76]
ATLAS Zjj 13 TeV $\Delta\phi_{jj}$ at 139 fb ⁻¹		12	Figure 7(d) of [109]

Table 2: Top physics observables from Tevatron and LHC Run I included in the fit.

Observables		no. of meas.	References
Top Data from Tevatron and LHC Run I		82	
Tevatron	forward-backward asymmetry $A_{FB}(m_{t\bar{t}})$ for $t\bar{t}$ production	4	[110]
ATLAS & CMS	charge asymmetry $A_C(m_{t\bar{t}})$ for $t\bar{t}$ production in the ℓ +jets channel.	6	[111]
	W -boson helicity fractions in top decay	3	[112]
ATLAS	charge asymmetry $A_C(m_{t\bar{t}})$ for $t\bar{t}$ production in the dilepton channel	1	[113]
	$\sigma_{t\bar{t}W}, \sigma_{t\bar{t}Z}$	2	[114]
	$\frac{d\sigma}{dp_t^T}, \frac{d\sigma}{dy_{t\bar{t}}}$ for t -channel single-top production	4 + 5	[115]
	σ_{tW} in the single lepton channel	1	[116]
	σ_{tW} in the dilepton channel	1	[117]
	s -channel single-top cross section	1	[118]
	$\frac{d\sigma}{dm_{t\bar{t}}}$ for $t\bar{t}$ production in the dilepton channel	6	[119]
	$\frac{d\sigma}{dp_t^T}$ for $t\bar{t}$ production in the ℓ +jets channel	8	[120]
CMS	$\sigma_{t\bar{t}\gamma}$ in the ℓ + jets channel.	1	[121]
	charge asymmetry $A_C(m_{t\bar{t}})$ for $t\bar{t}$ production in the dilepton channel.	3	[122]
	$\sigma_{t\bar{t}W}, \sigma_{t\bar{t}Z}$	2	[121]
	$\sigma_{t\bar{t}\gamma}$ in the ℓ + jets channel.	1	[123]
	s -channel single-top cross section	1	[124]
	$\frac{d\sigma}{dp_{t+\bar{t}}^T}$ of t -channel single-top production	6	[125]
	t -channel single-top and anti-top cross sections R_t .	1	[126]
	σ_{tW}	1	[127]
	$\frac{d\sigma}{dm_{t\bar{t}}dy_{t\bar{t}}}$ for $t\bar{t}$ production in the dilepton channel	16	[128, 129]
	$\frac{d\sigma}{dp_t^T}$ for $t\bar{t}$ production in the ℓ +jets channel	8	[130, 131]

Table 3: Top physics observables from LHC Run II included in the fit.

Observables		no. of meas.	References
Top Data from LHC Run II		55	
ATLAS	σ_{tW}	1	[132]
	σ_{tZ}	1	[133]
	$\sigma_{t+\bar{t}}$, R_t for t -channel single-top and anti-top cross sections	1+1	[134]
	charge asymmetry $A_C(m_{t\bar{t}})$ for $t\bar{t}$ production	5	[135]
	$\sigma_{t\bar{t}W}$, $\sigma_{t\bar{t}Z}$	2	[136]
	$\frac{d\sigma}{dp_T^\gamma}$ for $t\bar{t}\gamma$ production	11	[137]
CMS	σ_{tW}	1	[138]
	σ_{tZ} in the $Z \rightarrow \ell^+\ell^-$ channel	1	[139]
	$\frac{d\sigma}{dp_{t+\bar{t}}^T}$ and $R_t(p_{t+\bar{t}}^T)$ for t -channel single-top quark production	5 + 5	[140]
	$\frac{d\sigma}{dm_{t\bar{t}}}$ for $t\bar{t}$ production in the dilepton channel	6	[141]
	$\frac{d\sigma}{dm_{t\bar{t}}}$ for $t\bar{t}$ production in the ℓ +jets channel	15	[142]
	$\sigma_{t\bar{t}W}$	1	[143]
	$\frac{d\sigma}{dp_Z^T}$ for $t\bar{t}Z$ production	4	[144]

B Contributions to Z -pole observables in the LL approximation

In our global analysis, we assume flavor-universal ALP couplings. Here we provide the expressions for the SMEFT Wilson coefficients in the Warsaw basis [63] which enter Z -pole observables in the LL approximation in terms of the ALP coefficients in (4). Keeping only the entries $[\mathbf{Y}_u]_{33} \equiv y_t$, $[\mathbf{Y}_d]_{33} \equiv y_b$ and $[\mathbf{Y}_e]_{33} \equiv y_\tau$, the SMEFT Wilson coefficients at $\mu = m_Z$ read

$$\begin{aligned}
C_{HWB} &= 4 g_L g_Y C_{BB} C_{WW} \ln \frac{\Lambda}{m_Z}, \\
C_{HD} &= -\frac{8}{3} g_Y^2 C_{BB}^2 \ln \frac{\Lambda}{m_Z}, \\
[C_{Hq}^{(1)}]_{ij} &= \left[-\frac{4}{9} g_Y^2 C_{BB}^2 \delta_{ij} + \frac{1}{4} (y_t^2 C_u^2 - y_b^2 C_d^2) \delta_{i3} \delta_{j3} \right] \ln \frac{\Lambda}{m_Z}, \\
[C_{Hq}^{(3)}]_{ij} &= \left[-\frac{4}{3} g_L^2 C_{WW}^2 \delta_{ij} - \frac{1}{4} (y_t^2 C_u^2 + y_b^2 C_d^2) \delta_{i3} \delta_{j3} \right] \ln \frac{\Lambda}{m_Z}, \\
[C_{Hu}]_{ij} &= \left(-\frac{16}{9} g_Y^2 C_{BB}^2 \delta_{ij} - \frac{1}{2} y_t^2 C_u^2 \delta_{i3} \delta_{j3} \right) \ln \frac{\Lambda}{m_Z}, \\
[C_{Hd}]_{ij} &= \left(\frac{8}{9} g_Y^2 C_{BB}^2 \delta_{ij} + \frac{1}{2} y_b^2 C_d^2 \delta_{i3} \delta_{j3} \right) \ln \frac{\Lambda}{m_Z}, \\
[C_{Hud}]_{ij} &= y_b y_t C_d C_u \delta_{i3} \delta_{j3} \ln \frac{\Lambda}{m_Z}, \\
[C_{Hl}^{(1)}]_{ij} &= \left(\frac{4}{3} g_Y^2 C_{BB}^2 \delta_{ij} - \frac{1}{4} y_\tau^2 C_e^2 \delta_{i3} \delta_{j3} \right) \ln \frac{\Lambda}{m_Z}, \\
[C_{Hl}^{(3)}]_{ij} &= \left(-\frac{4}{3} g_L^2 C_{WW}^2 \delta_{ij} - \frac{1}{4} y_\tau^2 C_e^2 \delta_{i3} \delta_{j3} \right) \ln \frac{\Lambda}{m_Z}, \\
[C_{He}]_{ij} &= \left(\frac{8}{3} g_Y^2 C_{BB}^2 \delta_{ij} + \frac{1}{2} y_\tau^2 C_e^2 \delta_{i3} \delta_{j3} \right) \ln \frac{\Lambda}{m_Z}, \\
[C_{ll}]_{1221} &= -\frac{4}{3} g_L^2 C_{WW}^2 \ln \frac{\Lambda}{m_Z}, \tag{39}
\end{aligned}$$

where again $\Lambda = 4\pi f$, and the SMEFT Wilson coefficients normalized as C_i/Λ^2 . Parametrizing the Z and W coupling modifications as in [44], we obtain the following relations:

$$\begin{aligned}
\delta m_W^2 &= \frac{v^4}{\Lambda^2} \frac{g_Y^2 g_L^2}{g_L^2 - g_Y^2} \left(\frac{2}{3} C_{BB}^2 - 4 C_{BB} C_{WW} + C_{WW}^2 \right) \ln \frac{\Lambda}{m_Z}, \\
[\delta g_R^{Wq}]_{ij} &= -\frac{v^2}{\Lambda^2} \frac{y_b y_t}{2} C_d C_u \delta_{i3} \delta_{j3} \ln \frac{\Lambda}{m_Z}, \\
[\delta g_L^{Zu}]_{ij} &= \frac{v^2}{\Lambda^2} \left[\frac{\delta_{ij}}{g_L^2 - g_Y^2} \left(\frac{1}{9} g_Y^2 (5g_L^2 - g_Y^2) C_{BB}^2 - \frac{8}{3} g_L^2 g_Y^2 C_{BB} C_{WW} - \frac{1}{6} g_L^2 (g_L^2 - 5g_Y^2) C_{WW}^2 \right) \right. \\
&\quad \left. - \frac{\delta_{i3} \delta_{j3}}{4} y_t^2 C_u^2 \right] \ln \frac{\Lambda}{m_Z}, \\
[\delta g_L^{Zd}]_{ij} &= \frac{v^2}{\Lambda^2} \left[\frac{\delta_{ij}}{g_L^2 - g_Y^2} \left(-\frac{1}{9} g_Y^2 (g_L^2 + g_Y^2) C_{BB}^2 + \frac{4}{3} g_L^2 g_Y^2 C_{BB} C_{WW} + \frac{1}{6} g_L^2 (g_L^2 - 3g_Y^2) C_{WW}^2 \right) \right. \\
&\quad \left. + \frac{\delta_{i3} \delta_{j3}}{4} y_b^2 C_d^2 \right] \ln \frac{\Lambda}{m_Z},
\end{aligned}$$

$$\begin{aligned}
[\delta g_R^{Zu}]_{ij} &= \frac{v^2}{\Lambda^2} \left[\frac{g_Y^2}{g_L^2 - g_Y^2} \delta_{ij} \left(\frac{4}{9} (2g_L^2 - g_Y^2) C_{BB}^2 - \frac{8}{3} g_L^2 C_{BB} C_{WW} + \frac{2}{3} g_L^2 C_{WW}^2 \right) \right. \\
&\quad \left. + \frac{\delta_{i3} \delta_{j3}}{4} y_t^2 C_u^2 \right] \ln \frac{\Lambda}{m_Z}, \\
[\delta g_R^{Zd}]_{ij} &= \frac{v^2}{\Lambda^2} \left[\frac{g_Y^2}{g_L^2 - g_Y^2} \delta_{ij} \left(\frac{2}{9} (g_Y^2 - 2g_L^2) C_{BB}^2 + \frac{4}{3} g_L^2 C_{BB} C_{WW} - \frac{1}{3} g_L^2 C_{WW}^2 \right) \right. \\
&\quad \left. - \frac{\delta_{i3} \delta_{j3}}{4} y_b^2 C_d^2 \right] \ln \frac{\Lambda}{m_Z}, \\
[\delta g_L^{Wl}]_{ij} &= \frac{v^2}{\Lambda^2} \left[\frac{g_L^2}{g_L^2 - g_Y^2} \delta_{ij} \left(\frac{2}{3} g_Y^2 C_{BB}^2 - 4 g_Y^2 C_{BB} C_{WW} - \frac{1}{3} (g_L^2 - 4 g_Y^2) C_{WW}^2 \right) \right. \\
&\quad \left. - \frac{\delta_{i3} \delta_{j3}}{4} y_\tau^2 C_e^2 \right] \ln \frac{\Lambda}{m_Z}, \\
[\delta g_L^{Ze}]_{ij} &= \frac{v^2}{\Lambda^2} \left[\frac{\delta_{ij}}{g_L^2 - g_Y^2} \left(\frac{1}{3} g_Y^2 (g_Y^2 - 3g_L^2) C_{BB}^2 + 4 g_L^2 g_Y^2 C_{BB} C_{WW} + \frac{1}{6} g_L^2 (g_L^2 - 7g_Y^2) C_{WW}^2 \right) \right. \\
&\quad \left. + \frac{\delta_{i3} \delta_{j3}}{4} y_\tau^2 C_e^2 \right] \ln \frac{\Lambda}{m_Z}, \\
[\delta g_R^{Ze}]_{ij} &= \frac{v^2}{\Lambda^2} \left[\frac{g_Y^2}{g_L^2 - g_Y^2} \delta_{ij} \left(\frac{2}{3} (g_Y^2 - 2g_L^2) C_{BB}^2 + 4 g_L^2 C_{BB} C_{WW} - g_L^2 C_{WW}^2 \right) \right. \\
&\quad \left. - \frac{\delta_{i3} \delta_{j3}}{4} y_\tau^2 C_e^2 \right] \ln \frac{\Lambda}{m_Z}, \tag{40}
\end{aligned}$$

with the additional relations $\delta g_L^{Z\nu} = \delta g_L^{Ze} + \delta g_L^{Wl}$ and $\delta g_L^{Wq} \approx \delta g_L^{Zu} - \delta g_L^{Zd}$ (for $V_{\text{CKM}} \approx \mathbb{1}$). From these expressions it becomes clear why C_u remains unconstrained by Z -pole observables when working at LL accuracy, as this parameter only enters in $Zt\bar{t}$ coupling modifications.

References

- [1] R. D. Peccei and H. R. Quinn, *CP Conservation in the Presence of Instantons*, *Phys. Rev. Lett.* **38** (1977) 1440–1443.
- [2] S. Weinberg, *A New Light Boson?*, *Phys. Rev. Lett.* **40** (1978) 223–226.
- [3] F. Wilczek, *Problem of Strong P and T Invariance in the Presence of Instantons*, *Phys. Rev. Lett.* **40** (1978) 279–282.
- [4] F. Chadha-Day, J. Ellis and D. J. E. Marsh, *Axion dark matter: What is it and why now?*, *Sci. Adv.* **8** (2022) abj3618, [2105.01406].
- [5] B. Holdom and M. E. Peskin, *Raising the Axion Mass*, *Nucl. Phys. B* **208** (1982) 397–412.
- [6] J. M. Flynn and L. Randall, *A Computation of the Small Instanton Contribution to the Axion Potential*, *Nucl. Phys. B* **293** (1987) 731–739.
- [7] V. A. Rubakov, *Grand unification and heavy axion*, *JETP Lett.* **65** (1997) 621–624, [hep-ph/9703409].
- [8] Z. Berezhiani, L. Gianfagna and M. Giannotti, *Strong CP problem and mirror world: The Weinberg-Wilczek axion revisited*, *Phys. Lett. B* **500** (2001) 286–296, [hep-ph/0009290].
- [9] A. Hook, *Anomalous solutions to the strong CP problem*, *Phys. Rev. Lett.* **114** (2015) 141801, [1411.3325].
- [10] H. Fukuda, K. Harigaya, M. Ibe and T. T. Yanagida, *Model of visible QCD axion*, *Phys. Rev. D* **92** (2015) 015021, [1504.06084].
- [11] T. Gherghetta, N. Nagata and M. Shifman, *A Visible QCD Axion from an Enlarged Color Group*, *Phys. Rev. D* **93** (2016) 115010, [1604.01127].
- [12] S. Dimopoulos, A. Hook, J. Huang and G. Marques-Tavares, *A collider observable QCD axion*, *JHEP* **11** (2016) 052, [1606.03097].
- [13] P. Agrawal and K. Howe, *Factoring the Strong CP Problem*, *JHEP* **12** (2018) 029, [1710.04213].
- [14] M. K. Gaillard, M. B. Gavela, R. Houtz, P. Quilez and R. Del Rey, *Color unified dynamical axion*, *Eur. Phys. J. C* **78** (2018) 972, [1805.06465].
- [15] J. Fuentes-Martín, M. Reig and A. Vicente, *Strong CP problem with low-energy emergent QCD: The 4321 case*, *Phys. Rev. D* **100** (2019) 115028, [1907.02550].
- [16] T. Gherghetta, V. V. Khoze, A. Pomarol and Y. Shirman, *The Axion Mass from 5D Small Instantons*, *JHEP* **03** (2020) 063, [2001.05610].
- [17] A. Kivel, J. Laux and F. Yu, *Supersizing axions with small size instantons*, *JHEP* **11** (2022) 088, [2207.08740].
- [18] B. Gripaios, A. Pomarol, F. Riva and J. Serra, *Beyond the Minimal Composite Higgs Model*, *JHEP* **04** (2009) 070, [0902.1483].
- [19] G. Ferretti and D. Karateev, *Fermionic UV completions of Composite Higgs models*, *JHEP* **03** (2014) 077, [1312.5330].
- [20] A. E. Nelson and N. Seiberg, *R symmetry breaking versus supersymmetry breaking*, *Nucl. Phys. B* **416** (1994) 46–62, [hep-ph/9309299].
- [21] J. Bagger, E. Poppitz and L. Randall, *The R axion from dynamical supersymmetry breaking*, *Nucl. Phys. B* **426** (1994) 3–18, [hep-ph/9405345].

- [22] B. Bellazzini, A. Mariotti, D. Redigolo, F. Sala and J. Serra, *R-axion at colliders*, *Phys. Rev. Lett.* **119** (2017) 141804, [1702.02152].
- [23] D. Cadamuro and J. Redondo, *Cosmological bounds on pseudo Nambu-Goldstone bosons*, *JCAP* **02** (2012) 032, [1110.2895].
- [24] M. Millea, L. Knox and B. Fields, *New Bounds for Axions and Axion-Like Particles with keV-GeV Masses*, *Phys. Rev. D* **92** (2015) 023010, [1501.04097].
- [25] A. Payez, C. Evoli, T. Fischer, M. Giannotti, A. Mirizzi and A. Ringwald, *Revisiting the SN1987A gamma-ray limit on ultralight axion-like particles*, *JCAP* **02** (2015) 006, [1410.3747].
- [26] J. Jaeckel, P. C. Malta and J. Redondo, *Decay photons from the axionlike particles burst of type II supernovae*, *Phys. Rev. D* **98** (2018) 055032, [1702.02964].
- [27] K. Mimasu and V. Sanz, *ALPs at Colliders*, *JHEP* **06** (2015) 173, [1409.4792].
- [28] J. Jaeckel and M. Spannowsky, *Probing MeV to 90 GeV axion-like particles with LEP and LHC*, *Phys. Lett. B* **753** (2016) 482–487, [1509.00476].
- [29] S. Knapen, T. Lin, H. K. Lou and T. Melia, *Searching for Axionlike Particles with Ultraperipheral Heavy-Ion Collisions*, *Phys. Rev. Lett.* **118** (2017) 171801, [1607.06083].
- [30] I. Brivio, M. B. Gavela, L. Merlo, K. Mimasu, J. M. No, R. del Rey et al., *ALPs Effective Field Theory and Collider Signatures*, *Eur. Phys. J. C* **77** (2017) 572, [1701.05379].
- [31] M. Bauer, M. Neubert and A. Thamm, *Collider Probes of Axion-Like Particles*, *JHEP* **12** (2017) 044, [1708.00443].
- [32] M. Bauer, M. Heiles, M. Neubert and A. Thamm, *Axion-Like Particles at Future Colliders*, *Eur. Phys. J. C* **79** (2019) 74, [1808.10323].
- [33] B. Batell, M. Pospelov and A. Ritz, *Multi-lepton Signatures of a Hidden Sector in Rare B Decays*, *Phys. Rev. D* **83** (2011) 054005, [0911.4938].
- [34] M. Freytsis, Z. Ligeti and J. Thaler, *Constraining the Axion Portal with $B \rightarrow Kl^+l^-$* , *Phys. Rev. D* **81** (2010) 034001, [0911.5355].
- [35] M. J. Dolan, F. Kahlhoefer, C. McCabe and K. Schmidt-Hoberg, *A taste of dark matter: Flavour constraints on pseudoscalar mediators*, *JHEP* **03** (2015) 171, [1412.5174].
- [36] J. Martin Camalich, M. Pospelov, P. N. H. Vuong, R. Ziegler and J. Zupan, *Quark Flavor Phenomenology of the QCD Axion*, *Phys. Rev. D* **102** (2020) 015023, [2002.04623].
- [37] M. Bauer, M. Neubert, S. Renner, M. Schnubel and A. Thamm, *Axionlike Particles, Lepton-Flavor Violation, and a New Explanation of a_μ and a_e* , *Phys. Rev. Lett.* **124** (2020) 211803, [1908.00008].
- [38] M. Bauer, M. Neubert, S. Renner, M. Schnubel and A. Thamm, *Flavor probes of axion-like particles*, *JHEP* **09** (2022) 056, [2110.10698].
- [39] J. E. Kim, *Weak Interaction Singlet and Strong CP Invariance*, *Phys. Rev. Lett.* **43** (1979) 103.
- [40] M. A. Shifman, A. I. Vainshtein and V. I. Zakharov, *Can Confinement Ensure Natural CP Invariance of Strong Interactions?*, *Nucl. Phys. B* **166** (1980) 493–506.
- [41] M. Dine, W. Fischler and M. Srednicki, *A Simple Solution to the Strong CP Problem with a Harmless Axion*, *Phys. Lett. B* **104** (1981) 199–202.

- [42] A. R. Zhitnitsky, *On Possible Suppression of the Axion Hadron Interactions. (In Russian)*, *Sov. J. Nucl. Phys.* **31** (1980) 260.
- [43] A. M. Galda, M. Neubert and S. Renner, *ALP — SMEFT interference*, *JHEP* **06** (2021) 135, [2105.01078].
- [44] A. Falkowski, M. González-Alonso and K. Mimouni, *Compilation of low-energy constraints on 4-fermion operators in the SMEFT*, *JHEP* **08** (2017) 123, [1706.03783].
- [45] A. Biekötter, T. Corbett and T. Plehn, *The Gauge-Higgs Legacy of the LHC Run II*, *SciPost Phys.* **6** (2019) 064, [1812.07587].
- [46] E. da Silva Almeida, A. Alves, N. Rosa Agostinho, O. J. P. Éboli and M. C. Gonzalez-Garcia, *Electroweak Sector Under Scrutiny: A Combined Analysis of LHC and Electroweak Precision Data*, *Phys. Rev. D* **99** (2019) 033001, [1812.01009].
- [47] S. Brown, A. Buckley, C. Englert, J. Ferrando, P. Galler, D. J. Miller et al., *TopFitter: Fitting top-quark Wilson Coefficients to Run II data*, *PoS ICHEP2018* (2019) 293, [1901.03164].
- [48] N. P. Hartland, F. Maltoni, E. R. Nocera, J. Rojo, E. Slade, E. Vryonidou et al., *A Monte Carlo global analysis of the Standard Model Effective Field Theory: the top quark sector*, *JHEP* **04** (2019) 100, [1901.05965].
- [49] I. Brivio, S. Bruggisser, F. Maltoni, R. Moutafis, T. Plehn, E. Vryonidou et al., *O new physics, where art thou? A global search in the top sector*, *JHEP* **02** (2020) 131, [1910.03606].
- [50] S. Kraml, T. Q. Loc, D. T. Nhung and L. D. Ninh, *Constraining new physics from Higgs measurements with Lilith: update to LHC Run 2 results*, *SciPost Phys.* **7** (2019) 052, [1908.03952].
- [51] S. van Beek, E. R. Nocera, J. Rojo and E. Slade, *Constraining the SMEFT with Bayesian reweighting*, *SciPost Phys.* **7** (2019) 070, [1906.05296].
- [52] J. De Blas et al., *HEPfit: a code for the combination of indirect and direct constraints on high energy physics models*, *Eur. Phys. J. C* **80** (2020) 456, [1910.14012].
- [53] S. Dawson, S. Homiller and S. D. Lane, *Putting standard model EFT fits to work*, *Phys. Rev. D* **102** (2020) 055012, [2007.01296].
- [54] E. d. S. Almeida, A. Alves, O. J. P. Éboli and M. C. Gonzalez-Garcia, *Electroweak legacy of the LHC run II*, *Phys. Rev. D* **105** (2022) 013006, [2108.04828].
- [55] J. Ellis, M. Madigan, K. Mimasu, V. Sanz and T. You, *Top, Higgs, Diboson and Electroweak Fit to the Standard Model Effective Field Theory*, *JHEP* **04** (2021) 279, [2012.02779].
- [56] Anisha, S. Das Bakshi, S. Banerjee, A. Biekötter, J. Chakraborty, S. Kumar Patra et al., *Effective limits on single scalar extensions in the light of recent LHC data*, *Phys. Rev. D* **107** (2023) 055028, [2111.05876].
- [57] SMEFT collaboration, J. J. Ethier, G. Magni, F. Maltoni, L. Mantani, E. R. Nocera, J. Rojo et al., *Combined SMEFT interpretation of Higgs, diboson, and top quark data from the LHC*, *JHEP* **11** (2021) 089, [2105.00006].
- [58] S. Iranipour and M. Ubiali, *A new generation of simultaneous fits to LHC data using deep learning*, *JHEP* **05** (2022) 032, [2201.07240].
- [59] S. Bruggisser, D. van Dyk and S. Westhoff, *Resolving the flavor structure in the MFV-SMEFT*, *JHEP* **02** (2023) 225, [2212.02532].

- [60] V. Bresó-Pla, A. Falkowski, M. González-Alonso and K. Monsálvez-Pozo, *EFT analysis of New Physics at COHERENT*, *JHEP* **05** (2023) 074, [2301.07036].
- [61] Z. Kassabov, M. Madigan, L. Mantani, J. Moore, M. Morales Alvarado, J. Rojo et al., *The top quark legacy of the LHC Run II for PDF and SMEFT analyses*, *JHEP* **05** (2023) 205, [2303.06159].
- [62] C. Grunwald, G. Hiller, K. Kröninger and L. Nollen, *More Synergies from Beauty, Top, Z and Drell-Yan Measurements in SMEFT*, 2304.12837.
- [63] B. Grzadkowski, M. Iskrzynski, M. Misiak and J. Rosiek, *Dimension-Six Terms in the Standard Model Lagrangian*, *JHEP* **10** (2010) 085, [1008.4884].
- [64] M. Bauer, M. Neubert, S. Renner, M. Schnubel and A. Thamm, *The Low-Energy Effective Theory of Axions and ALPs*, *JHEP* **04** (2021) 063, [2012.12272].
- [65] J. Elias-Miro, J. R. Espinosa, E. Masso and A. Pomarol, *Higgs windows to new physics through $d=6$ operators: constraints and one-loop anomalous dimensions*, *JHEP* **11** (2013) 066, [1308.1879].
- [66] E. E. Jenkins, A. V. Manohar and M. Trott, *Renormalization Group Evolution of the Standard Model Dimension Six Operators I: Formalism and lambda Dependence*, *JHEP* **10** (2013) 087, [1308.2627].
- [67] E. E. Jenkins, A. V. Manohar and M. Trott, *Renormalization Group Evolution of the Standard Model Dimension Six Operators II: Yukawa Dependence*, *JHEP* **01** (2014) 035, [1310.4838].
- [68] R. Alonso, E. E. Jenkins, A. V. Manohar and M. Trott, *Renormalization Group Evolution of the Standard Model Dimension Six Operators III: Gauge Coupling Dependence and Phenomenology*, *JHEP* **04** (2014) 159, [1312.2014].
- [69] M. Chala, G. Guedes, M. Ramos and J. Santiago, *Running in the ALPs*, *Eur. Phys. J. C* **81** (2021) 181, [2012.09017].
- [70] J. Bonilla, I. Brivio, M. B. Gavela and V. Sanz, *One-loop corrections to ALP couplings*, *JHEP* **11** (2021) 168, [2107.11392].
- [71] S. Das Bakshi, J. Machado-Rodríguez and M. Ramos, *Running beyond ALPs: shift-breaking and CP-violating effects*, 2306.08036.
- [72] A. Celis, J. Fuentes-Martin, A. Vicente and J. Virto, *DsixTools: The Standard Model Effective Field Theory Toolkit*, *Eur. Phys. J. C* **77** (2017) 405, [1704.04504].
- [73] J. Fuentes-Martin, P. Ruiz-Femenia, A. Vicente and J. Virto, *DsixTools 2.0: The Effective Field Theory Toolkit*, *Eur. Phys. J. C* **81** (2021) 167, [2010.16341].
- [74] ATLAS collaboration, *Interpretations of the combined measurement of Higgs boson production and decay*, *ATLAS-CONF-2020-053* (10, 2020) .
- [75] A. Efrati, A. Falkowski and Y. Soreq, *Electroweak constraints on flavorful effective theories*, *JHEP* **07** (2015) 018, [1503.07872].
- [76] CMS collaboration, A. M. Sirunyan et al., *Measurements of production cross sections of the Higgs boson in the four-lepton final state in proton–proton collisions at $\sqrt{s} = 13$ TeV*, *Eur. Phys. J. C* **81** (2021) 488, [2103.04956].
- [77] A. Mariotti, D. Redigolo, F. Sala and K. Tobioka, *New LHC bound on low-mass diphoton resonances*, *Phys. Lett. B* **783** (2018) 13–18, [1710.01743].

- [78] J. Bonilla, I. Brivio, J. Machado-Rodríguez and J. F. de Trocóniz, *Nonresonant searches for axion-like particles in vector boson scattering processes at the LHC*, *JHEP* **06** (2022) 113, [2202.03450].
- [79] M. B. Gavela, J. M. No, V. Sanz and J. F. de Trocóniz, *Nonresonant Searches for Axionlike Particles at the LHC*, *Phys. Rev. Lett.* **124** (2020) 051802, [1905.12953].
- [80] S. Carra, V. Goumarre, R. Gupta, S. Heim, B. Heinemann, J. Kuechler et al., *Constraining off-shell production of axionlike particles with $Z\gamma$ and WW differential cross-section measurements*, *Phys. Rev. D* **104** (2021) 092005, [2106.10085].
- [81] CMS collaboration, A. Tumasyan et al., *Search for heavy resonances decaying to ZZ or ZW and axion-like particles mediating nonresonant ZZ or ZH production at $\sqrt{s} = 13$ TeV*, *JHEP* **04** (2022) 087, [2111.13669].
- [82] G. Alonso-Álvarez, M. B. Gavela and P. Quilez, *Axion couplings to electroweak gauge bosons*, *Eur. Phys. J. C* **79** (2019) 223, [1811.05466].
- [83] F. Esser, M. Madigan, V. Sanz and M. Ubiali, *On the coupling of axion-like particles to the top quark*, 2303.17634.
- [84] BABAR collaboration, J. P. Lees et al., *Search for a Dark Photon in e^+e^- Collisions at BaBar*, *Phys. Rev. Lett.* **113** (2014) 201801, [1406.2980].
- [85] G. Lucente and P. Carena, *Supernova bound on axionlike particles coupled with electrons*, *Phys. Rev. D* **104** (2021) 103007, [2107.12393].
- [86] R. Essig, R. Harnik, J. Kaplan and N. Toro, *Discovering New Light States at Neutrino Experiments*, *Phys. Rev. D* **82** (2010) 113008, [1008.0636].
- [87] A. Biekötter, M. Chala and M. Spannowsky, *New Higgs decays to axion-like particles*, *Phys. Lett. B* **834** (2022) 137465, [2203.14984].
- [88] F. Arias-Aragón, J. Quevillon and C. Smith, *Axion-like ALPs*, *JHEP* **03** (2023) 134, [2211.04489].
- [89] L. Di Luzio, F. Mescia and E. Nardi, *Window for preferred axion models*, *Phys. Rev. D* **96** (2017) 075003, [1705.05370].
- [90] J. Fuentes-Martín, M. König, J. Pagès, A. E. Thomsen and F. Wilsch, *A Proof of Concept for Matchete: An Automated Tool for Matching Effective Theories*, 2212.04510.
- [91] K. Choi, S. H. Im, C. B. Park and S. Yun, *Minimal Flavor Violation with Axion-like Particles*, *JHEP* **11** (2017) 070, [1708.00021].
- [92] G. Alonso-Álvarez, F. Ertas, J. Jaeckel, F. Kahlhoefer and L. J. Thormaehlen, *Leading logs in QCD axion effective field theory*, *JHEP* **07** (2021) 059, [2101.03173].
- [93] L. Allwicher, P. Arnan, D. Barducci and M. Nardecchia, *Perturbative unitarity constraints on generic Yukawa interactions*, *JHEP* **10** (2021) 129, [2108.00013].
- [94] ATLAS, CMS collaboration, G. Aad et al., *Measurements of the Higgs boson production and decay rates and constraints on its couplings from a combined ATLAS and CMS analysis of the LHC pp collision data at $\sqrt{s} = 7$ and 8 TeV*, *JHEP* **08** (2016) 045, [1606.02266].
- [95] ATLAS collaboration, G. Aad et al., *Measurements of the Higgs boson production and decay rates and coupling strengths using pp collision data at $\sqrt{s} = 7$ and 8 TeV in the ATLAS experiment*, *Eur. Phys. J. C* **76** (2016) 6, [1507.04548].
- [96] ATLAS collaboration, G. Aad et al., *A search for the $Z\gamma$ decay mode of the Higgs boson in pp collisions at $\sqrt{s} = 13$ TeV with the ATLAS detector*, 2005.05382.

- [97] ATLAS collaboration, G. Aad et al., *A search for the dimuon decay of the Standard Model Higgs boson with the ATLAS detector*, *Phys. Lett. B* **812** (2021) 135980, [2007.07830].
- [98] ATLAS COLLABORATION collaboration, *Measurements of Higgs boson production cross-sections in the $H \rightarrow \tau^+\tau^-$ decay channel in pp collisions at $\sqrt{s} = 13$ TeV with the ATLAS detector*, tech. rep., CERN, Geneva, Aug, 2021.
- [99] ATLAS collaboration, G. Aad et al., *Measurements of Higgs bosons decaying to bottom quarks from vector boson fusion production with the ATLAS experiment at $\sqrt{s} = 13$ TeV*, *Eur. Phys. J. C* **81** (2021) 537, [2011.08280].
- [100] ATLAS collaboration, *Measurement of the Higgs boson decaying to b-quarks produced in association with a top-quark pair in pp collisions at $\sqrt{s} = 13$ TeV with the ATLAS detector*, *ATLAS-CONF-2020-058* (11, 2020) .
- [101] ATLAS collaboration, *Measurements of gluon fusion and vector-boson-fusion production of the Higgs boson in $H \rightarrow WW^* \rightarrow e\nu\mu\nu$ decays using pp collisions at $\sqrt{s} = 13$ TeV with the ATLAS detector*, *ATLAS-CONF-2021-014* (3, 2021) .
- [102] CMS collaboration, *Combined Higgs boson production and decay measurements with up to 137 fb⁻¹ of proton-proton collision data at $\sqrt{s} = 13$ TeV*, *CMS-PAS-HIG-19-005* (2020) .
- [103] CMS collaboration, A. M. Sirunyan et al., *Measurement of the inclusive and differential Higgs boson production cross sections in the leptonic WW decay mode at $\sqrt{s} = 13$ TeV*, *JHEP* **03** (2021) 003, [2007.01984].
- [104] CMS collaboration, A. M. Sirunyan et al., *Evidence for Higgs boson decay to a pair of muons*, *JHEP* **01** (2021) 148, [2009.04363].
- [105] CMS collaboration, A. M. Sirunyan et al., *Measurement of the Higgs boson production rate in association with top quarks in final states with electrons, muons, and hadronically decaying tau leptons at $\sqrt{s} = 13$ TeV*, *Eur. Phys. J. C* **81** (2021) 378, [2011.03652].
- [106] CMS collaboration, *Measurement of Higgs boson production in association with a W or Z boson in the $H \rightarrow WW$ decay channel*, *CMS-PAS-HIG-19-017* (2021) .
- [107] CMS collaboration, *Measurement of Higgs boson production in the decay channel with a pair of τ leptons*, *CMS-PAS-HIG-19-010* (2020) .
- [108] CMS collaboration, A. M. Sirunyan et al., *Measurements of Higgs boson production cross sections and couplings in the diphoton decay channel at $\sqrt{s} = 13$ TeV*, *JHEP* **07** (2021) 027, [2103.06956].
- [109] ATLAS collaboration, G. Aad et al., *Differential cross-section measurements for the electroweak production of dijets in association with a Z boson in proton–proton collisions at ATLAS*, *Eur. Phys. J. C* **81** (2021) 163, [2006.15458].
- [110] CDF, D0 collaboration, T. A. Aaltonen et al., *Combined Forward-Backward Asymmetry Measurements in Top-Antitop Quark Production at the Tevatron*, *Phys. Rev. Lett.* **120** (2018) 042001, [1709.04894].
- [111] ATLAS, CMS collaboration, M. Aaboud et al., *Combination of inclusive and differential $t\bar{t}$ charge asymmetry measurements using ATLAS and CMS data at $\sqrt{s} = 7$ and 8 TeV*, *JHEP* **04** (2018) 033, [1709.05327].
- [112] CMS, ATLAS collaboration, G. Aad et al., *Combination of the W boson polarization measurements in top quark decays using ATLAS and CMS data at $\sqrt{s} = 8$ TeV*, *JHEP* **08** (2020) 051, [2005.03799].

- [113] ATLAS collaboration, G. Aad et al., *Measurements of the charge asymmetry in top-quark pair production in the dilepton final state at $\sqrt{s} = 8$ TeV with the ATLAS detector*, *Phys. Rev. D* **94** (2016) 032006, [1604.05538].
- [114] ATLAS collaboration, G. Aad et al., *Measurement of the $t\bar{t}W$ and $t\bar{t}Z$ production cross sections in pp collisions at $\sqrt{s} = 8$ TeV with the ATLAS detector*, *JHEP* **11** (2015) 172, [1509.05276].
- [115] ATLAS collaboration, M. Aaboud et al., *Fiducial, total and differential cross-section measurements of t -channel single top-quark production in pp collisions at 8 TeV using data collected by the ATLAS detector*, *Eur. Phys. J. C* **77** (2017) 531, [1702.02859].
- [116] ATLAS collaboration, G. Aad et al., *Measurement of single top-quark production in association with a W boson in the single-lepton channel at $\sqrt{s} = 8$ TeV with the ATLAS detector*, *Eur. Phys. J. C* **81** (2021) 720, [2007.01554].
- [117] ATLAS collaboration, G. Aad et al., *Measurement of the production cross-section of a single top quark in association with a W boson at 8 TeV with the ATLAS experiment*, *JHEP* **01** (2016) 064, [1510.03752].
- [118] ATLAS collaboration, G. Aad et al., *Evidence for single top-quark production in the s -channel in proton-proton collisions at $\sqrt{s} = 8$ TeV with the ATLAS detector using the Matrix Element Method*, *Phys. Lett. B* **756** (2016) 228–246, [1511.05980].
- [119] ATLAS collaboration, M. Aaboud et al., *Measurement of top quark pair differential cross-sections in the dilepton channel in pp collisions at $\sqrt{s} = 7$ and 8 TeV with ATLAS*, *Phys. Rev. D* **94** (2016) 092003, [1607.07281].
- [120] ATLAS collaboration, G. Aad et al., *Measurements of top-quark pair differential cross-sections in the lepton+jets channel in pp collisions at $\sqrt{s} = 8$ TeV using the ATLAS detector*, *Eur. Phys. J. C* **76** (2016) 538, [1511.04716].
- [121] CMS collaboration, V. Khachatryan et al., *Observation of top quark pairs produced in association with a vector boson in pp collisions at $\sqrt{s} = 8$ TeV*, *JHEP* **01** (2016) 096, [1510.01131].
- [122] CMS collaboration, V. Khachatryan et al., *Measurements of $t\bar{t}$ charge asymmetry using dilepton final states in pp collisions at $\sqrt{s} = 8$ TeV*, *Phys. Lett. B* **760** (2016) 365–386, [1603.06221].
- [123] CMS collaboration, A. M. Sirunyan et al., *Measurement of the semileptonic $t\bar{t} + \gamma$ production cross section in pp collisions at $\sqrt{s} = 8$ TeV*, *JHEP* **10** (2017) 006, [1706.08128].
- [124] CMS collaboration, V. Khachatryan et al., *Search for s channel single top quark production in pp collisions at $\sqrt{s} = 7$ and 8 TeV*, *JHEP* **09** (2016) 027, [1603.02555].
- [125] CMS collaboration, *Single top t -channel differential cross section at 8 TeV*, .
- [126] CMS collaboration, V. Khachatryan et al., *Measurement of the t -channel single-top-quark production cross section and of the $|V_{tb}|$ CKM matrix element in pp collisions at $\sqrt{s} = 8$ TeV*, *JHEP* **06** (2014) 090, [1403.7366].
- [127] CMS collaboration, S. Chatrchyan et al., *Observation of the associated production of a single top quark and a W boson in pp collisions at $\sqrt{s} = 8$ TeV*, *Phys. Rev. Lett.* **112** (2014) 231802, [1401.2942].
- [128] CMS collaboration, A. M. Sirunyan et al., *Measurement of double-differential cross sections for top quark pair production in pp collisions at $\sqrt{s} = 8$ TeV and impact on parton distribution functions*, *Eur. Phys. J. C* **77** (2017) 459, [1703.01630].

- [129] CMS collaboration, S. Chatrchyan et al., *Measurement of the $t\bar{t}$ production cross section in the dilepton channel in pp collisions at $\sqrt{s} = 8$ TeV*, *JHEP* **02** (2014) 024, [1312.7582].
- [130] CMS collaboration, V. Khachatryan et al., *Measurement of the differential cross section for top quark pair production in pp collisions at $\sqrt{s} = 8$ TeV*, *Eur. Phys. J. C* **75** (2015) 542, [1505.04480].
- [131] CMS collaboration, V. Khachatryan et al., *Measurements of the $t\bar{t}$ production cross section in lepton+jets final states in pp collisions at 8 TeV and ratio of 8 to 7 TeV cross sections*, *Eur. Phys. J. C* **77** (2017) 15, [1602.09024].
- [132] ATLAS collaboration, M. Aaboud et al., *Measurement of the cross-section for producing a W boson in association with a single top quark in pp collisions at $\sqrt{s} = 13$ TeV with ATLAS*, *JHEP* **01** (2018) 063, [1612.07231].
- [133] ATLAS collaboration, M. Aaboud et al., *Measurement of the production cross-section of a single top quark in association with a Z boson in proton–proton collisions at 13 TeV with the ATLAS detector*, *Phys. Lett. B* **780** (2018) 557–577, [1710.03659].
- [134] ATLAS collaboration, M. Aaboud et al., *Measurement of the inclusive cross-sections of single top-quark and top-antiquark t-channel production in pp collisions at $\sqrt{s} = 13$ TeV with the ATLAS detector*, *JHEP* **04** (2017) 086, [1609.03920].
- [135] ATLAS collaboration, *Inclusive and differential measurement of the charge asymmetry in $t\bar{t}$ events at 13 TeV with the ATLAS detector*, .
- [136] ATLAS collaboration, M. Aaboud et al., *Measurement of the $t\bar{t}Z$ and $t\bar{t}W$ cross sections in proton-proton collisions at $\sqrt{s} = 13$ TeV with the ATLAS detector*, *Phys. Rev. D* **99** (2019) 072009, [1901.03584].
- [137] ATLAS collaboration, G. Aad et al., *Measurements of inclusive and differential cross-sections of combined $t\bar{t}\gamma$ and $tW\gamma$ production in the $e\mu$ channel at 13 TeV with the ATLAS detector*, *JHEP* **09** (2020) 049, [2007.06946].
- [138] CMS collaboration, A. M. Sirunyan et al., *Measurement of the production cross section for single top quarks in association with W bosons in proton-proton collisions at $\sqrt{s} = 13$ TeV*, *JHEP* **10** (2018) 117, [1805.07399].
- [139] CMS collaboration, A. M. Sirunyan et al., *Observation of Single Top Quark Production in Association with a Z Boson in Proton-Proton Collisions at $\sqrt{s} = 13$ TeV*, *Phys. Rev. Lett.* **122** (2019) 132003, [1812.05900].
- [140] CMS collaboration, A. M. Sirunyan et al., *Measurement of differential cross sections and charge ratios for t-channel single top quark production in proton–proton collisions at $\sqrt{s} = 13$ TeV*, *Eur. Phys. J. C* **80** (2020) 370, [1907.08330].
- [141] CMS collaboration, A. M. Sirunyan et al., *Measurement of the $t\bar{t}$ production cross section, the top quark mass, and the strong coupling constant using dilepton events in pp collisions at $\sqrt{s} = 13$ TeV*, *Eur. Phys. J. C* **79** (2019) 368, [1812.10505].
- [142] CMS collaboration, *Measurement of differential $t\bar{t}$ production cross sections in the full kinematic range using lepton+jets events from pp collisions at $\sqrt{s} = 13$ TeV*, .
- [143] CMS collaboration, A. M. Sirunyan et al., *Measurement of the cross section for top quark pair production in association with a W or Z boson in proton-proton collisions at $\sqrt{s} = 13$ TeV*, *JHEP* **08** (2018) 011, [1711.02547].

- [144] CMS collaboration, A. M. Sirunyan et al., *Measurement of top quark pair production in association with a Z boson in proton-proton collisions at $\sqrt{s} = 13$ TeV*, *JHEP* **03** (2020) 056, [[1907.11270](#)].